MASTER: Macroscopic Traffic Simulation Based on A Gas-Kinetic, Non-Local Traffic Model

Dirk Helbing, Ansgar Hennecke, Vladimir Shvetsov, and Martin Treiber
II. Institute of Theoretical Physics, University of Stuttgart,
Pfaffenwaldring 57, D-70550 Stuttgart, Germany
(Submitted September 3, 1998; revised February 28, 1999)

We present a gas-kinetic ("Boltzmann-like") traffic equation that is not only suited for low vehicle densities, but also for the high-density regime, as it takes into account the forwardly directed interactions, effects of vehicular space requirements like increased interaction rates, and effects of velocity correlations that reflect the bunching of cars, at least partially. From this gas-kinetic equation, we systematically derive the related macroscopic traffic equations.

The corresponding partial differential equations for the vehicle density and average velocity are directly related to the quantities characterizing individual driver-vehicle behavior, and, as we show by calibration of the model, their optimal values have the expected order of magnitude. Therefore, the model allows to investigate the influences of varying street and weather conditions or freeway control measures. We point out that, because of the forwardly directed interactions, the macroscopic equations contain non-local instead of diffusion or viscosity terms. This resolves some of the inconsistencies found in previous models and allows for a fast and robust numerical integration, so that several thousand freeway kilometers can be simulated in real-time.

It turns out that the model is in good agreement with the experimentally observed properties of freeway traffic flow. In particular, it reproduces the characteristic outflow and dissolution velocity of traffic jams, as well as the phase transition to "synchronized" congested traffic. We also reproduce the five different kinds of congested states that have been found close to on-ramps (or bottlenecks) and present a "phase diagram" of the different traffic states in dependence of the main flow and the ramp flow, showing that congested states are often induced by perturbations in the traffic flow. Finally, we introduce generalized macroscopic equations for multi-lane and multi-userclass traffic. With these, we investigate the differences between multi-lane simulations and simulations of the effective one-lane model.

I. INTRODUCTION

In recent years, the community of scientists engaged in traffic modelling (for overviews see Leutzbach, 1988; Helbing, 1997a; Schreckenberg/Wolf 1998) is rapidly growing. This is not only due to its practical implications for optimizing freeway traffic (Bovy, 1998), but also because of the observed non-equilibrium phase transitions (Kerner/Rehborn, 1997; Helbing/Huberman, 1998) and the various non-linear dynamical phenomena like the formation of traffic jams (Kerner/Konhäuser, 1993), stop-and-go traffic (Kühne, 1984, 1987; Kerner/Konhäuser, 1994), and "synchronized" congested traffic (Kerner/Rehborn, 1996b, 1997; Helbing/Treiber, 1998b). It seems that all forms of congested traffic have almost universal properties which are largely independent of the initial conditions and the spatially averaged density, like the characteristic outflow $Q_{\rm out}$ from traffic jams of about 1800 ± 200 vehicles per hour and lane or their typical dissolution velocity C of about -15 ± 5 kilometers per hour (Kerner/Rehborn 1996a). This universality arises from the highly correlated state of motion produced by traffic congestions (Kerner, 1997). In particular, the outflow $Q_{\rm out}$ is related to the time gap between successive departures from the traffic jam. Therefore, the outflow is practically independent of the initial conditions and the kind

of congested traffic. As a consequence of the constant outflow, the propagation velocity C of jam fronts, given by the dissolution speed of traffic jams, is nearly constant as well.

II. MACROSCOPIC TRAFFIC MODELS

A. State-of-the-Art

As a consequence of the conservation of the number of vehicles, all macroscopic traffic models are based on the continuity equation

$$\frac{\partial \rho}{\partial t} + \frac{\partial (\rho V)}{\partial x} = \nu(x,t) \tag{1}$$

for the vehicle density $\rho(x,t)$ at position x and time t. $\nu(x,t)$ reflects the rate of vehicles entering or leaving the freeway at on- or off-ramps. The differences between the various existing macroscopic traffic models concern the equation for the average vehicle velocity $V(x,t)$. The Lighthill-Whitham model (Lighthill/Whitham, 1955; Richards, 1956) and its variants (Newell 1993a, b, c; Daganzo 1994, 1995a; Hilliges/Weidlich 1995; Lebacque, 1997) assume the equilibrium relation $V(x,t) = V_{\rm e}(\rho(x,t))$. For the description of emergent traffic jams and stop-and-go traffic, however, one needs a dynamic velocity equation. Most proposals can (in their continuous form) be summarized by the velocity equation

$$\frac{\partial V}{\partial t} + \underbrace{V\frac{\partial V}{\partial x}}_{\text{Transport Term}} = \underbrace{-\frac{1}{\rho}\frac{\partial P}{\partial x}}_{\text{Pressure Term}} + \underbrace{\frac{1}{\tau}(V_{\rm e} - V)}_{\text{Relaxation Term}} . \tag{2}$$

Their main difference is the specification of the traffic pressure P, the relaxation time τ, and the dynamic equilibrium velocity $V_{\rm e}$, which is dependent on the local vehicle density ρ. Notice that the Lighthill-Whitham model results in the limit $\tau \to 0$. Payne's (1971) and Papageorgiou's (1983) model is obtained for $P(\rho) = [V_0 - V_{\rm e}(\rho)]/(2\tau)$, with the "free" or "desired" average velocity $V_0 = V_{\rm e}(0)$. For $dP/d\rho = -\rho/[2\tau(\rho+\kappa)]dV_{\rm e}/d\rho$, one ends up at Cremer's (1979) model. In the model of Phillips (1979), there is $P = \rho\theta$, where θ denotes the velocity variance. The model of Kühne (1984, 1987), Kerner and Konhäuser (1993) results for $P = \rho\theta_0 - \eta\partial V/\partial x$, where θ_0 is a positive constant and η a viscosity coefficient. In comparison with a similar model by Whitham (1974), the additional contribution $-\eta\partial V/\partial x$ implies a viscosity term $(\eta/\rho)\,\partial^2 V/\partial x^2$. This is essential for smoothing shock fronts, which is desireable from an empirical and a numerical point of view.

B. Discussion

Many of the above mentioned models have proved their value in various applications, but they have been seriously criticized by Daganzo (1995b) because of theoretical inconsistencies. Apart from that, it is hard to decide which model is the best one. Whereas classical approaches focussed on reproducing the empirically observed velocity-density relation and the regime of unstable traffic flow, recent publications pointed out that it is more important to have traffic models which are able to describe the observed spectrum of non-linear phenomena and their characteristic properties (Kerner/Konhäuser, 1993, 1994; Kerner/Rehborn 1996a; Bando, 1995; Treiber/Hennecke/Helbing, 1999; Helbing/Schreckenberg, 1999). We think that it would be desireable to develop models that reproduce both aspects of empirical data. In the following, we will propose such a macroscopic traffic model, which is theoretically consistent as well (Helbing, 1996a, b).

III. THE NON-LOCAL, GAS-KINETIC-BASED TRAFFIC MODEL

A. Underlying Gas-Kinetic Traffic Flow Theory

In order to have meaningful and measurable model parameters, our macroscopic model of uni-directional freeway traffic was derived from a gas-kinetic traffic equation (Helbing, 1996a, b, 1997; Helbing/Treiber 1998a) that was systematically obtained from a "microscopic" description of driver vehicle behavior (Helbing, 1997a; Treiber/Hennecke/Helbing 1999). Gas-kinetic (i.e. Boltzmann-like) traffic models have already been proposed in a number of previous publications (Prigogine, 1971; Paveri-Fontana, 1975; Phillips, 1979; Nelson, 1995), but the correct treatment of the most interesting regime of moderate and high densities was still an open problem. In some recent references (Helbing 1996b; Wagner *et al.*, 1996; Klar/Wegener, 1997), the effect of vehicular space requirements has been taken into account by an additional factor χ reflecting the increased interaction rate of vehicles, however, still applying the so-called "vehicular chaos assumption" which assumes that the velocities of successive vehicles are uncorrelated. In the following, we will show how Prigogine's Boltzmann-like interaction term can be generalized in a way that allows to treat correlated and extended vehicles at high traffic densities.

Let us start with writing down the gas-kinetic traffic equation for the so-called phase-space density

$$f(x,v,t) = \rho(x,t)d(v;x,t), \tag{3}$$

which describes the spatial vehicle density $\rho(x,t)$ at location x and time t, multiplied with the spatio-temporal distribution $d(v;x,t)$ of individual vehicle velocities v. Postponing the treatment of the multi-userclass case to Section III F, we will assume that all vehicles have the same desired velocity V_0 (which approximately reflects the situation of freeways with a speed limit of V_0). According to Paveri-Fontana (1975), who removed some inconsistencies of Prigogine's (1971) Boltzmann-like model (arising from his approach for the acceleration term), the spatio-temporal evolution of the phase-space density obeys the so-called *continuity equation*

$$\frac{\partial f}{\partial t} = -\frac{\partial}{\partial x}\left(f\frac{dx}{dt}\right) - \frac{\partial}{\partial v}\left(f\frac{dv}{dt}\right), \tag{4}$$

describing the conservation of the number of vehicles in the absence of on- and off-ramps (see also Helbing, 1997a). This equation states that the temporal change $\partial f/\partial t$ of f is determined by changes dx/dt of the vehicle position x in time, which are given by the equation of motion,

$$\frac{dx}{dt} = v(t)\,, \tag{5}$$

and by continuous changes dv/dt of the velocity v, reflecting the acceleration and deceleration behavior of vehicles. Often one assumes

$$\frac{dv}{dt} = \frac{V_0 - v(t)}{\tau} - h(\Delta x, v, \Delta v) + \xi(t)\,. \tag{6}$$

Herein, the acceleration term

$$\left(\frac{dv}{dt}\right)_{\rm acc} = \frac{V_0 - v}{\tau} \tag{7}$$

describes an (exponential) adaptation of the actual vehicle velocity v to the desired velocity V_0 with a relaxation time τ, that may depend on the vehicle density. Note that, although this term is quite realistic, an even better agreement with reality may be obtained by the formula $V_0(1 - v/V_0)^\delta/\tau$ with $\delta \geq 1$ (Treiber/Helbing, 1999b). The white noise $\xi(t)$ obeying $\langle\xi\rangle = 0$ and $\langle\xi(t)\xi(t') = 2D\delta(t-t')\rangle$ reflects individual

velocity variations due to imperfect driving and other effects. This gives rise to a velocity-diffusion term of the form

$$\left(\frac{df}{dt}\right)_{\text{diff}} = \frac{\partial^2}{\partial v^2}(fD)\,. \tag{8}$$

Later on, it will lead to the finite velocity variance $\theta = D\tau$ of vehicles [equation (32)], which is even observed in the presence of speed limits and small vehicle densities [Figure 1(a)].

Finally, the function h describes the braking behavior of vehicles. It depends on the distance Δx to the next vehicle, the velocity difference Δv, and the own velocity v. In gas-kinetic models, one usually assumes an instantaneous braking to the velocity $w < v$ of the slower vehicle in front, if overtaking is not possible. This approximation of the deceleration behavior is justified only, because braking (lasting for some seconds) happens on a much faster time scale than the macroscopic traffic dynamics (being of the order of minutes, as exemplified by the time interval between successive stop-and-go waves). It simplifies the calculations considerably, leading to the Boltzmann-like braking interaction term

$$\begin{aligned}\left(\frac{df}{dt}\right)_{\text{int}} &= (1-p') \int\limits_{w>v} dw\,(w-v) f_2(x,w,x',v,t) \\ &\quad - (1-p') \int\limits_{w<v} dw\,(v-w) f_2(x,v,x',w,t)\,,\end{aligned} \tag{9}$$

where the probability of undelayed overtaking is reflected by the density-dependent function p'. Whereas the last term of (9) describes the temporal decrease of the phase-space density $f(x,v,t)$ related to vehicles around location x with velocity w that decelerate to the velocity $w < v$ of slower vehicles around location x', the previous term delineates the increase of the phase-space density due to deceleration of fast vehicles with velocity $w > v$ around location x to the velocity v of vehicles around location x'. Choosing $x' = (x + s)$ with $s > 0$ will allow us to consider the fact that vehicle interactions are forwardly directed, since drivers mainly react to the traffic situation at some "interaction point" x' in front of them. The shift s mainly reflects the velocity-dependent safe distance, which will be specified later.

According to formula (9), the interaction rate of vehicles is, as usual, proportional to the relative velocity $|v - w|$ and to the so-called pair-distribution function f_2 of vehicles. Prigogine (1971) and Paveri-Fontana (1975) assumed point-like vehicles with uncorrelated velocities, which results in the factorization

$$f_2(x,v,x',w,t) = f(x,v,t) f(x',w,t) = \rho(x,t)\rho(x',t) d(v;x,t) d(w;x,t) \tag{10}$$

("vehicular chaos assumption"). However, this assumption is valid only at small densities. At higher densities, we must take into account the increase of the interaction rate by a density-dependent factor $\chi' \geq 1$, since the proportion $1/\chi' \geq 0$ of free space is reduced by the vehicular space requirements. For simplicity, we will assume that the overtaking probability is just given by this proportion of free space, i.e.

$$p' = 1/\chi'\,. \tag{11}$$

At high vehicle densities, the velocities of successive cars will additionally by correlated. This is particularly clear for vehicle platoons (Islam/Consul, 1991), in which the variation of vehicle velocities is considerably reduced (close to zero). There have been several suggestions for the treatment of vehicle platoons (Andrews, 1970, 1973a, b; Beylich, 1979, 1981). Related to an approach by Lampis (1978) and others (Poethke, 1982, see Leutzbach, 1988; Hoogendoorn/Bovy, 1998), one possibility is to distinguish a fraction $c(\rho)$ of free vehicles and a fraction $[1 - c(\rho)]$ of bound (i.e. obstructed) vehicles (Helbing, 1997d). In the resulting effective equations for traffic composed of free and bound vehicles, one will get a density-dependent relaxation time

$\tau(\rho) = \tau(0)/c(\rho)$. This reflects the so-called "frustration effect" that $\tau(\rho)$ increases with density due to the decrease of $c(\rho)$, consequences of which are discussed later on (see Figures 6 and 12). The most realistic description of vehicle platoons, however, is to set up equations for vehicle clusters of different sizes (Beylich, 1979, 1981). Unfortunately, this ends up with a very complex hierarchy of spatio-temporal equations, from which useful macroscopic equations have not yet been successfully derived. Therefore, we propose a simplified but quite realistic way of describing the relevant aspects of obstructed vehicle motion. For this, let $r \geq 0$ denote the correlation coefficient of successive vehicle velocities, which we expect to increase continuously with vehicle density. Taking also into account the fact that empirical vehicle velocities are more or less Gaussian distributed (Pampel, 1955; Gerlough/Huber, 1975; May, 1990; Helbing, 1997c), we will approximate the two-vehicle velocity-distribution function by a bivariate Gaussian function

$$d_2(v,w) = \frac{\sqrt{\det\, B}}{2\pi}\, \mathrm{e}^{-B(v,w)/2} \tag{12}$$

with the quadratic form

$$B(v,w) = \frac{1}{1-r^2}\left(\frac{(v-V)^2}{\theta} - 2r\frac{(v-V)(w-V')}{\sqrt{\theta\theta'}} + \frac{(w-V')}{\theta'}\right) \tag{13}$$

and its determinant

$$\det\, B = \frac{1}{\theta\theta'(1-r^2)}\,. \tag{14}$$

Herein, V denotes the average velocity and θ the velocity variance of vehicles around location x at time t, whereas the variables with a prime refer to the location x' of the advanced interaction point.

Summarizing the above consideration, a good approximation for the pair distribution function at high vehicle densities is given by

$$f_2(x,v,x',w,t) = \rho(x,t)\rho(x',t)d_2(v,w;x,x',t)\,, \tag{15}$$

and the resulting improved gas-kinetic traffic equation reads

$$\frac{\partial f}{\partial t} = -\frac{\partial}{\partial x}\,(fv) - \frac{\partial}{\partial v}\left(f\frac{V_0-v}{\tau}\right) + \frac{\partial^2}{\partial v^2}(fD) + (1-p')\chi'\rho(x,t)\rho(x',t)\left[\int\limits_{w>v} dw\,(w-v)d_2(w,v) - \int\limits_{w<v} dw\,(v-w)d_2(v,w)\right]. \tag{16}$$

B. Derivation of the Macroscopic Model

The macroscopic traffic equations related to the above gas-kinetic traffic model can be obtained by multiplying equation (16) with v^k ($k \in \{0,1,2\}$) and subsequent integration over v. The results are expressed in terms of aggregate ("macroscopic") quantities, namely the spatial vehicle density

$$\rho(x,t) = \int dv\; f(x,v,t)\,, \tag{17}$$

the average velocity

$$V(x,t) = \frac{1}{\rho(x,t)}\int dv\; v\, f(x,v,t) = \int dv\, v\, d(v;x,t)\,, \tag{18}$$

and the velocity variance

$$\theta(x,t) = \frac{1}{\rho(x,t)} \int dv\, [v - V(x,t)]^2 f(x,v,t) = \int dv\, [v - V(x,t)]^2 d(v;x,t)\,. \quad (19)$$

The corresponding calculations are more or less straightforward, but very lengthy and rather difficult. In deriving the associated macroscopic equations, different approximations have been suggested, the most harmless of which was a gradient expansion (Helbing, 1996a). This lead to a viscosity term and some unexpected but essential high-density corrections containing spatial derivatives of different orders. However, the resulting traffic dynamics did not agree with real traffic

Meanwhile we managed to evaluate the Boltzmann-like gas-kinetic interaction term exactly (Helbing, 1998; Helbing/Treiber, 1998a; Treiber/Hennecke/Helbing, 1999), even with inclusion of velocity correlations among successive vehicles (Shvetsov/Helbing, 1999). The results will be given below. They can be written in the general form of the continuity equation (1) and the velocity equation (2), but with a non-local, *dynamical* equilibrium velocity V_e that depends on the vehicle density and other aggregate quantities at the actual vehicle location x and at the advanced "interaction point" x':

$$V_e = V_0 - \underbrace{\tau[1 - p(\rho')]\chi(\rho')\rho' B(\Delta V)}_{\text{Braking Term}}\,. \quad (20)$$

This implies that V_e implicitly depends on the gradients of macroscopic variables like the density. Again, a prime indicates that the corresponding variable is taken at the interaction point $x' = (x + s)$ rather than at the actual position x. For simplicity, we have assumed the safe distance s to increase linearly with the average vehicle velocity V:

$$s = \gamma \left(\frac{1}{\rho_{\max}} + TV \right)\,, \quad (21)$$

where $\rho_{\max}$ denotes the maximum vehicle density, $T \approx 1.8\,\mathrm{s}$ the safe time headway, and $\gamma \approx 1$ an anticipation factor.

The "Boltzmann factor"

$$B(\Delta V) = S\left\{\Delta V N(\Delta V) + [1 + (\Delta V)^2]E(\Delta V)\right\}\,, \quad (22)$$

in which

$$N(y) = \frac{\mathrm{e}^{-y^2/2}}{\sqrt{2\pi}} \quad (23)$$

represents the normal distribution and

$$E(y) = \int_{-\infty}^{y} dz\, \frac{\mathrm{e}^{-z^2/2}}{\sqrt{2\pi}} \quad (24)$$

the Gaussian error function, describes the dependence of the braking interaction on the effective dimensionless difference ΔV between the velocities at the actual position and the interaction point. The effective velocity difference is defined by

$$\Delta V = \frac{V - V'}{\sqrt{S}}\,, \quad (25)$$

where

$$S = \theta - 2r\sqrt{\theta\theta'} + \theta'\,. \quad (26)$$

Hence, apart from the velocity difference to the interaction point, ΔV takes also into account the velocity variance θ at the actual vehicle position x, the velocity variance θ' at the interaction point x', and the correlation r among successive cars. In homogeneous traffic, we have $B(0) = S/2$. In the limiting case $\Delta V \gg 0$, where the preceding cars are much slower, we have a much stronger interaction $B(\Delta V) = (\Delta V)^2 S$. If, in contrast, the preceding cars are much faster (i.e. $\Delta V \ll 0$), we have $B(\Delta V) \approx 0$. That is, since the distance is increasing, then, the vehicle will not brake, even if its headway is smaller than the safe distance.

Notice that, for $\gamma = 1$, the macroscopic interaction term can be easily understood by the underlying microscopic dynamics of the gas-kinetic-based traffic model. If a vehicle at location x with velocity v is faster than one at x' with velocity w (i.e. $\Delta v = v - w > 0$), it approaches the car in front within the time $\Delta t = \Delta x_{\rm free}/\Delta v$, where $\Delta x_{\rm free} = 1/(\rho'\chi')$ is the average interaction-free distance per car. Then, if it cannot overtake immediately, which would happen with probability $(1 - p')$, it abruptly reduces the velocity by Δv. The resulting ensemble-averaged deceleration is

$$\langle \Delta v/\Delta t \rangle = -(1-p')\chi'\rho' \int_0^\infty d(\Delta v)\ (\Delta v)^2 d_\Delta(\Delta v)\,. \tag{27}$$

If v and w are Gaussian distributed with averages V, V' and variances θ, θ', respectively, with a correlation r, the distribution function $d_\Delta(\Delta v)$ of the velocity difference Δv is Gaussian distributed, with expectation value $V - V' = \sqrt{S}\,\Delta V$ and variance S. Evaluating integral (27) yields $\langle \Delta v/\Delta t \rangle = -(1-p')\chi'\rho' B(\Delta V)$, i.e., the macroscopic braking term in equation (20).

Next, we will specify the pressure relation. Similar to gases, the calculations give

$$P = \rho[\theta + W(\rho)] \tag{28}$$

(Helbing, 1997a, d). Again,

$$\theta = \langle \theta_i \rangle = \sum_{i=1}^{I} \frac{\rho_i}{I\rho}\,\theta_i \tag{29}$$

is the (weighted) average of the lane-specific velocity variances θ_i, where the weights are the relative densities $\rho_i/(I\rho)$ in the I different lanes i. The monotonically decreasing, density-dependent function

$$W = \langle (V_i - V)^2 \rangle = \sum_{i=1}^{I} \frac{\rho_i}{I\rho}(V_i)^2 - \left(\sum_{i=1}^{I} \frac{\rho_i}{I\rho} V_i \right)^2 \tag{30}$$

can be used to correct for the variation of the average velocities V_i in the different lanes [Figure 8(a)], but it is often neglected.

The pressure term describes the kinematic dispersion of the macroscopic velocity in inhomogeneous traffic as a consequence of the finite velocity variance. For example, the macroscopic velocity in front of a small vehicle cluster will increase *even if no individual vehicle accelerates*, because the faster cars will leave the cluster behind. The kinematic dispersion also leads to a smooth density profile at the dissolution front between congested traffic and an empty road, as it occurs when a road blockage is removed (cf. Figure 2).

Notice that the total variance

$$\Theta = (\theta + W) \tag{31}$$

decreases with density and vanishes at the maximum vehicle density $\rho_{\rm max}$. Therefore, the density-gradient $dP/d\rho$ of the traffic pressure P may decrease with growing density and increase with decreasing density. Hence, according to the pressure term $-(1/\rho)\partial P/\partial x$, it seems that vehicles would accelerate into denser regions and

decelerate when driving into regions of lighter traffic. This tendency, however, is overcompensated for by the non-local interaction term (Helbing, 1996b). Because of its non-locality, the braking term in relation (20) strongly increases with the density gradient. This can be more explicitly seen by applying the gradient expansions $\rho' \approx \rho + s\,\partial\rho/\partial x + \ldots$ etc.

Next, in order to close the system of equations, one needs to specify the dynamics of the velocity variance θ and the correlation coefficient r. Since r is difficult to obtain and has not yet been determined from empirical data, with some exceptions (Nelson, 1995; Klar/Wegener, 1997) one usually assumes $r = 0$. Nevertheless, the above formulas allow us to estimate the changes by a finite velocity correlation $r \neq 0$, which can be the consequence of the formation of platoons. This would only modify the equilibrium velocity a bit, similar to a reduction of velocity variances. Furthermore, it turned out that, for a description of the presently known properties of traffic flows, we do not need to describe the variance by the associated partial differential equation. It seems sufficient to describe the variance by the equilibrium relation

$$\theta = D\tau \tag{32}$$

of the dynamical variance equation (Helbing, 1997b). Empirical data (Helbing, 1996b; Treiber/Hennecke/Helbing, 1999) suggest that the variance is a density-dependent fraction $\alpha(\rho)$ of the squared average velocity,

$$\theta = \alpha(\rho)V^2\,, \tag{33}$$

which guarantees that the velocity variance will vanish if the average velocity goes to zero, as required. It turns out that the variance prefactor α is higher in congested traffic than in free traffic. The empirical data can be approximated by the Fermi function

$$\alpha(\rho) = \alpha_0 + \Delta\alpha\left[\tanh\left(\frac{\rho-\rho_c}{\Delta\rho}\right)+1\right], \tag{34}$$

where α_0 and $\alpha_0 + 2\Delta\alpha$ are about the variance prefactors for free and congested traffic, respectively, ρ_c is of the order of the critical density for the transition from free to congested traffic, and $\Delta\rho$ denotes the width of the transition.

Finally, we will specify the "effective cross section" $(1-p)\chi = (1-p)/p$ so that the average time headway of vehicles corresponds to the safe time headway T, if the vehicle density is high (i.e. the freeway space is almost used up completely by the vehicular space requirements). This specification means that, in dense and homogeneous traffic situations with $V' = V$ and $\theta' = \theta$, we should have $s = 1/\rho = [1/\rho_{\max} + TV_e(\rho)]$, where we insert the equilibrium solution (36). This gives us the relation

$$[1-p(\rho)]\chi(\rho) = \frac{V_0\rho T^2}{\tau\alpha(\rho_{\max})(1-\rho/\rho_{\max})^2}\,, \tag{35}$$

which makes also sense in the low-density limit $\rho \to 0$, since it implies $\chi \to 1$ and $p \to 1$.

C. Properties of the Non-Local, Gas-Kinetic-Based Traffic Model

Summarizing the above results, our gas-kinetic-based traffic model can be written in the general form (1), (2) of macroscopic traffic models, but with a non-local relaxation term. Since the equations are structurally related to, for example, the Kerner-Konhäuser model (1993), we find many similar non-linear phenomena (Treiber/Hennecke/Helbing, 1999). This includes the sequence of stable, linearly unstable, and metastable regimes (Kerner/Konhäuser, 1994; Kerner/Konhäuser/Schilke, 1996), the local breakdown effect (Kerner/Konhäuser/Schilke, 1995), the local cluster effect (Kerner/Konhäuser,

1994), and, at sufficiently large densities, the formation of dipole layers (Kerner/Konhäuser/Schilke, 1996). The response of equilibrium traffic to localized disturbances is similar to the Kerner-Konhäuser model (Kerner/Konhäuser/Schilke, 1995). More specific, for densities below a certain critical density ρ_{c1} and above some density ρ_{c4}, homogeneous traffic is stable with respect to localized perturbations [Figure 3(a)+(d)], and for a range $\rho_{c2} < \rho < \rho_{c3}$ of intermediate densities, it is linearly unstable, giving rise to cascades of traffic jams ["stop-and-go traffic", cf. Figure 3(c)]. For the two density regimes $\rho_{c1} \leq \rho \leq \rho_{c2}$ and $\rho_{c3} \leq \rho \leq \rho_{c4}$ between the stable and the linearly unstable regions, traffic is metastable, i.e., it behaves unstable with respect to perturbations exceeding a certain critical amplitude $\Delta\rho_{cr}(\rho)$ [Figure 3(b)], but otherwise stable. For the self-organized density ρ_{jam} inside traffic jams we find a typical value $\rho_{jam} > \rho_{c4}$ (Treiber/Hennecke/Helbing, 1999). Furthermore, there exists a range $\rho_{cv} < \rho < \rho_{c3}$ with $\rho_{cv} > \rho_{c2}$, where traffic is linearly unstable, but convectively stable, i.e., all perturbations grow, but they are eventually convected away in upstream direction (Cross/Hohenberg, 1993).

In addition, we obtain that, in the unstable traffic regime, the resulting flow-density relation differs from the equilibrium one (lying below the latter). We also find that the outflow Q_{out} from traffic jams is independent of the initial conditions and the spatially averaged density [Figure 4(a)]. Furthermore, the dissolution velocity C of traffic jams varies only a little with density [Figure 4(b)].

The main difference with respect to other macroscopic traffic models is the non-local character of the braking term. Nevertheless, our model can still be rewritten in form of flux equations, with a non-local source term (Helbing, 1998; Helbing/Treiber, 1998a). For this reason, we can apply various standard methods of numerical integration. It turns out that the non-local term has similar smoothing properties like a viscosity term, but its effect is anisotropic. There is no smoothing in forward direction (cf. Figure 5), which would imply that vehicles would react on density or velocity gradients behind them. Compared to a viscosity term, the non-locality does not change the hyperbolic character of the partial differential equations to a parabolic one, and it has favourable properties with respect to numerical stability and integration speed. Therefore, our model allows a robust real-time simulation of freeway stretches up to several thousand kilometers on a usual PC.

D. Model Calibration and Validation

It turns out that our model can be easily calibrated to the static and dynamic properties of traffic flow data by a systematic procedure. In homogeneous traffic, the average velocity relaxes to

$$V_e(\rho) = \frac{\tilde{V}^2}{2V_0}\left(-1 \pm \sqrt{1+\frac{4V_0^2}{\tilde{V}^2}}\right) \tag{36}$$

with

$$\tilde{V}(\rho) = \frac{1}{T}\left(\frac{1}{\rho} - \frac{1}{\rho_{max}}\right)\sqrt{\frac{\alpha(\rho_{max})}{\alpha(\rho)}}\,. \tag{37}$$

This also determines the equilibrium traffic flow by

$$Q_e(\rho) = \rho V_e(\rho). \tag{38}$$

In the limit of small densities we find $V_e(\rho) \approx V_0$, while in the limit of high densities (i.e. for $(1-\rho/\rho_{max}) \ll 1$ or $V_e \ll V_0$), we have $V_e(\rho) \approx (1/\rho - 1/\rho_{max})/T$. Apparently, the equilibrium flow-density relation is only affected by the model parameters V_0, T, and ρ_{max}. The desired velocity V_0 can be determined by fitting flow-density data at low densities by a straight line ρV_0. While the safe time headway T and the

maximum density $\rho_{\max}$ are obtained by fitting the data at high densities by a straight line $(1-\rho/\rho_{\max})/T$, which crosses the abszissa at $\rho_{\max}$ with a slope of $-1/(\rho_{\max}T)$.

The model parameters τ and γ influence the stability behavior. Figure 6 shows that an increased value of τ leads both to an increased range of *instability*, and to increased amplitudes $(\rho_{\rm jam}-\rho_{\min})$ of traffic jams. Further simulations showed that higher values of γ tend to increase the *stability* of traffic. This is plausible, since γ reflects the anticipation of future velocity changes. γ and τ also determine the shape and width of the downstream and upstream fronts connecting free and congested states (cf. Figures 2 and 5). Since τ and γ weakly influence the outflow $Q_{\rm out}$ from traffic jams, the calibration of T, τ, and γ is repeated recursively until an optimal fit of the model to the empirical data is obtained.

Because of their intuitive meaning, the plausible range of values for the model parameters is rather restricted. V_0 is given by the average free speed. $\rho_{\max}$ must be consistent with the average length of vehicles plus a reasonable bumper-to-bumper distance of about 1.5 m in standing traffic. T should be compatible with the average time headway kept in homogeneous congested traffic (Kerner, 1997; Raub/Pfefer, 1998). Reasonable time headways are in the range $T\in[1.0\text{s}, 2.5\text{s}]$. Initial accelerations $a_{\max}=V_0/\tau$ are typically in the range $a_{\max}\in[1\ \text{m/s}^2, 4\ \text{m/s}^2]$, corresponding to $\tau\in[10\,\text{s}, 40\,\text{s}]$. (Notice that, for $V_0=158$ km/h, τ would have the meaning of the average acceleration time from 0 to 100 km/h.) Therefore, a relaxation time $\tau\approx 35\,\text{s}$ is reasonable for freeway traffic, whereas τ is smaller for city traffic. Finally, the minimum anticipation of traffic is to the car in front, implying $\gamma\geq 1$.

The above procedure of parameter calibration has been applied to single-vehicle data of the Dutch freeway A9, leading to the parameter set shown in Table I. It turns out that all optimized parameters have realistic values. In particular, this holds for τ. The typical values for the safe time headway of $T=1.8\,\text{s}$ is consistent with the rule "distance (in m) should not be less than half the velocity (in km/h)" suggested by German road authorities. For other data, however, one often finds that a somewhat smaller time headway yields a better fit.

Since the model parameters are meaningful, it is simple to model changes of the traffic dynamics caused by external effects like environmental influences (cf. Figure 7). For example, a speed limit would be considered by decreasing V_0. Bad weather conditions leading to more defensive driving would be characterized by an increased time headway T and a lower value of V_0 (plus a reduction of γ, if there is heavy fog). In rush-hour traffic, it is plausible to assume a higher percentage of experienced drivers than in holiday traffic, which would correspond to a higher γ. Effects like a varying distribution of vehicle types can be modelled as well. For example, a higher proportion of trucks would lead to a decrease of V_0 and $\rho_{\max}$, but also to an increased value of τ.

E. Simulation Results

1. Synchronized Congested Traffic

Recently, Kerner and Rehborn (1997) have presented experimental data indicating a first-order transition to "synchronized" congested traffic. Traffic data from several freeways in Germany (Kerner/Rehborn, 1996b, 1997), the Netherlands (Helbing, 1997a, b; Treiber/Helbing, 1999a), and the United States (Daganzo *et al.*, 1998) indicate that synchronized traffic is the most common form of congested traffic. Synchronized traffic typically occurs at on-ramps when vehicles are added to already busy "freeways" and has the following properties: (i) The dynamics of the average velocities on all lanes is highly correlated ("synchronized"). (ii) The corresponding points in the flow-density plane are widely scattered. (iii) Synchronized traffic is characterized by a low average velocity, but, in contrast to traffic jams, the associated traffic flow is rather high. (iv) The transition to synchronized traffic is often caused by a localized and short perturbation of traffic flow that starts downstream of the on-ramp

and propagates upstream with a velocity of about $-10\,\mathrm{km/h}$. (v) As soon as the perturbation passes the on-ramp, it triggers synchronized traffic which spreads upstream in the course of time. (vi) Downstream, synchronized traffic eventually relaxes to free traffic. (vii) Synchronized traffic often persists over several hours. (viii) The transition from synchronized traffic to free traffic occurs at a lower density and higher average velocity than the inverse transition *(hysteresis effect).*

We believe that property (i), i.e. the synchronization among lanes, occurs automatically when there is a transition to congested traffic, because the velocity difference among lanes is negligible at densities of 30 vehicles per kilometer and lane or above [Figure 8(a)]. This is related to the fact that drivers change lanes if they can increase their speed by doing so, which can be described by a multi-lane model (see Sec. III F).

Property (ii) seems to be the result of the diversity of vehicles (Treiber/Helbing, 1999a), as demonstrated in Figure 8(b). The other characteristic properties of "synchronized" traffic can be reproduced by the effective one-lane version of the non-local, gas-kinetic-based traffic model described above. The only additional point is that, along on-ramps (or off-ramps), the source term

$$\nu = \frac{Q_{\mathrm{rmp}}}{nL} \tag{39}$$

is given by the actually observed inflow $Q_{\mathrm{rmp}} > 0$ from (or outflow $Q_{\mathrm{rmp}} < 0$ to) the ramp, divided by the merging length L and by the number n of lanes. The inflow has an upper limit that depends on the downstream flow on the main road (Daganzo, 1998). If the average velocity V_{rmp} of entering or leaving vehicles on the ramp is different from the average velocity V on the main road, this gives an additional contribution

$$\frac{\nu}{\rho}(V_{\mathrm{rmp}} - V) \tag{40}$$

to the velocity equation (2), corresponding to a source term νV_{rmp} in the related differential equation for the traffic flow $Q = \rho V$ on the freeway (Helbing, 1997d). However, usually one assumes $V_{\mathrm{rmp}} \approx V$.

Our simulations reproduced the observations (iii) to (viii) very realistically. For $V_{\mathrm{rmp}} = V$, the parameter values $V_0 = 128\,\mathrm{km/h}$, $\rho_{\max} = 160\,\mathrm{vehicles/km}$, $T = 1.6\,\mathrm{s}$, $\tau = 31\,\mathrm{s}$, $\gamma = 1.0$, and the observed boundary flows [Figure 9(c)], the simulated velocities and flows are, apart from fluctuations, in good agreement with the empirical curves presented by Kerner and Rehborn (1997) (Helbing/Treiber, 1998b).

Our results suggest the following interpretation of the phase transition to "synchronized" congested traffic: Initially, the homogeneous flow Q_{main} upstream of an on-ramp is stable, while the higher downstream flow $Q_{\mathrm{down}} = Q_{\mathrm{main}} + Q_{\mathrm{rmp}}/n$ is metastable. Without any disturbance of the main or ramp flow, free traffic flow will continue. However, a (positive or even a negative) perturbation in the on-ramp or the main flow will eventually cause a breakdown of velocity close to the on-ramp. Speaking in the terminology of Daganzo, Cassidy, and Bertini (1998), the perturbation will eventually "activate the bottleneck" associated with the on-ramp. In the following, we will explain and quantify the mechanism of this transition.

According to Figure 9, the perturbation triggers a stop-and-go wave, which travels downstream as long as it is small and upstream as it becomes larger, as is known from "localized clusters" (Kerner/Konhäuser/Schilke, 1995). Now, assume the downstream front of the cluster would pass the on-ramp. Then, since Q_{main} [Figure 9(c)] is lower than the characteristic outflow Q_{out} from a jam, the cluster would eventually vanish. However, during its lifetime, the cluster would continue to emit the flow Q_{out}, leading downstream of the ramp to a flow $Q_{\mathrm{out}} + Q_{\mathrm{rmp}}/n > Q_{\max}$. As a consequence, as soon as the perturbation reaches the on-ramp, it induces congested traffic with a *standing* downstream front just at the end of the ramp. With an observed outflow $\tilde{Q}_{\mathrm{out}} \lesssim Q_{\mathrm{out}}$ from synchronized traffic, the average flow upstream is given by

$$Q_{\mathrm{sync}} = \tilde{Q}_{\mathrm{out}} - Q_{\mathrm{rmp}}/n\,. \tag{41}$$

Hence, the congested region upstream the on-ramp is growing as long as the flow $Q_{\rm main}$ from the main road drops below $Q_{\rm sync}$. Only then, the congested region starts to "melt", and it can easily take an additional hour or so until traffic returns to free flow, even if the maximum flow $Q_{\rm max}$ has never been exceeded by $(Q_{\rm main} + Q_{\rm rmp}/n)$!

Now, consider the density $\rho_{\rm sync}$ defined by $Q_{\rm sync} = Q_{\rm e}(\rho_{\rm sync})$ in the congested part of the equilibrium flow-density relation $Q_{\rm e}(\rho)$ (i.e. behind its maximum). If homogeneous traffic is (meta-)stable at $\rho_{\rm sync}$, the on-ramp induces "synchronized" congested traffic. The restriction $Q_{\rm rmp} \leq \tilde{Q}_{\rm out}/2$ (Daganzo, 1998) implies $Q_{\rm sync} \geq \tilde{Q}_{\rm out}(1 - \frac{1}{2n})$ and $\rho_{\rm sync} < \rho_{\rm jam}$, so that "synchronized" congested flow is significantly higher than the flow inside traffic jams.

2. A Phase Diagram of Traffic States at Bottlenecks

Close to bottlenecks by on-ramps, lane closures, gradients, or other effects (including building sites along the road, bad street conditions, curves, accidents in the opposite lanes, and slow vehicles), there can develop a variety of different traffic states. Free traffic (FT) and the above discussed type of "synchronized" congested traffic, which we will also call "homogeneous congested traffic" (HCT) [Figure 10(a)], are only two of them. Other congested traffic states that can emerge are "oscillating congested traffic" (OCT), "triggered stop-and-go waves" (TSG), "moving localized clusters" (MLC) and "pinned (standing) localized clusters" (PLC). All these different congested states are observable in empirical traffic data (Kerner/Rehborn, 1996a, b, 1997; Helbing, 1997b; Kerner, 1998; Daganzo *et al.*, 1998), although the "synchronized" congested states have sometimes be interpreted differently in the beginning.

In our traffic simulations, we found out that most of the congested traffic states occur below the capacity limit $Q_{\rm max}$, and they are triggered by perturbations in traffic flow. This is only possible since the outflow $Q_{\rm out}$ from traffic jams is an additional, self-organized capacity limit, which is smaller than $Q_{\rm max}$ (due to the larger time headways occuring in accelerating traffic). The same fact brings about that most breakdowns of traffic flow could be avoided by control measures which manage to suppress these perturbations.

Our simulations also indicate that the conditions, under which the different traffic states appear, are clearly defined (Helbing/Treiber, 1998c; Helbing/Hennecke/Treiber, 1998). This is illustrated by the phase diagram in Figure 11, displaying the traffic states as a function of the main flow $Q_{\rm main}$ and the on-ramp flow per freeway lane, $Q_{\rm rmp}/n$ (which is a measure of the flow reduction by a bottleneck). It explains why usually not all possible congested traffic states are observed at every bottleneck, but only a typical, site-specific subset of them. The phase diagram also allows to understand the various observed transitions between the traffic states, which correspond to crossing the phase boundaries separating the different states. Notice that these phase boundaries can be calculated analytically in terms of the flows $Q_{{\rm c}i} = Q_{\rm e}(\rho_{{\rm c}i})$ characterizing the stability diagram (see Section III C). This implies that the general structure of the phase diagram in Figure 11 is expected to be *universal* for all microscopic and macroscopic traffic models which possess the same instability diagram (i.e. the sequence of stable, metastable, unstable, convectively stable, metastable, and stable traffic with increasing density). Only the exact position and the shape of the phase boundaries will vary from one model to another. Note, however, that the phase diagram in Figure 11 is for fully developed perturbations. For smaller perturbations, the phase boundaries will be shifted. The MLC and PLC regimes may even disappear, leading to the boundaries FT↔TSG, FT↔OCT, and FT↔HCT. In any case, there are regions of multistability, where the resulting traffic state depends on the initial condition.

Finally, we give a qualitative interpretation of the transitions between the various congested traffic states and the respective conditions, under which they appear. For example, the transition HCT→OCT from homogeneous to oscillating congested traffic occurs, when the ramp flow $Q_{\rm rmp}$ is decreased so that the synchronized flow (41)

falls into the unstable density regime instead of the (meta-)stable one. A further decrease in the ramp flow will reduce the average density in the congested region so much that we will have an alternation between regimes of free and congested traffic, which defines stop-and-go waves. We call them triggered stop-and-go waves (TSG) because, whenever an upstream travelling jam passes the bottleneck, it triggers a small perturbation which travels downstream as long as it is small, but eventually changes its speed as it grows and changes its propagation direction. Finally, the developed perturbation travels upstream and passes the bottleneck, where it gives birth to a new perturbation, and so on.

Obviously, the small triggered perturbation cannot grow, when the traffic flow downstream of the bottleneck is (meta-)stable, which will lead to a single localized cluster (LC). The localized cluster will pass the bottleneck in upstream direction (MLC), if traffic flow is unstable or metastable, there. In contrast, the localized cluster will be pinned at the bottleneck (PLC), if traffic in the upstream region is stable, since a density cluster could not survive, there. If the traffic flow downstream of the bottleneck is also stable, only free traffic (FT) can persist. Finally, the pinned localized cluster will grow to an extended region of congested traffic, if its outflow $\tilde{Q}_{\rm out}$ is smaller than the flow $(Q_{\rm main} + Q_{\rm rmp}/n)$ downstream of the bottleneck.

3. Transitions from Free to Synchronized and Stop-and-Go Traffic

Kerner (1998) has recently described the detailled features of a transition from "synchronized" congested traffic to stop-and-go patterns on German highways, which has been also observed on Dutch highways (Helbing, 1997b). In the following, we suggest a quantitative explanation of these observations (Treiber/Helbing, 1999b). In particular, we will show the possible coexistence of different traffic states along the road behind an inhomogeneity of traffic flow. It is, in upstream direction, associated with the sequence homogeneous congested traffic → oscillating congested traffic (which Kerner calls the "pinch region") → stop-and-go waves, while we have free traffic flow downstream of the inhomogeneity. We believe that this phenomenon should be triggered at relatively small bottlenecks whenever traffic flow $Q_{\rm main}(t)$ exceeds the flow $Q_{\rm c1} = Q_{\rm e}(\rho_{\rm c1})$ that characterizes the transition to metastable traffic flow.

The necessary conditions for this phenomenon are a metastability of traffic flow, a density inside of traffic jams that is much larger than in "synchronized" congested traffic, and a sufficiently large density regime of linearly unstable traffic flow that is convectively stable: If a linearly unstable kind of "synchronized" congested traffic has formed, small perturbations will eventually grow to larger oscillations, which propagate in upstream direction faster than the congested region grows. When the oscillations reach the region of free traffic upstream of the bottleneck, which we require to be metastable, oscillations with an amplitude below the critical amplitude $\Delta\rho_{\rm cr}(\rho_{\rm main})$ will eventually disappear, whereas the remaining ones will continue to grow until they are fully developed traffic jams (see Figure 12). We point out that a sequence of such jams is sustained, because the propagation velocity C and the outflow $Q_{\rm out} \approx Q_{\rm e}(\rho_{\rm c1})$ from jams are characteristic constants (see Section III C).

To maintain this mechanism, the homogeneous region of "synchronized" congested traffic upstream of the bottleneck must persist (i.e. it must not dissolve to stop-and-go waves). This is only the case, if traffic flow is convectively stable, there, i.e. if any perturbations propagate exlusively in upstream direction, so that they are convected away from the bottleneck. In order to reach this large convectively stable regime and a density inside of traffic jams that is much larger than in typical "synchronized" congested traffic, we had to include in our model a density-dependence of the relaxation time, reflecting the frustration effect mentioned in Section III A. We have chosen the relation

$$\tau(\rho) = \tau(0)\,\frac{1+\exp[(\rho_{\rm c}^* - \rho)/\Delta\rho^*]}{1-u+\exp[(\rho_{\rm c}^* - \rho)/\Delta\rho^*]}\,, \qquad (42)$$

which is applied in equation (20), whereas in the term V/τ of Eq. (2) we insert for τ the value $\tau(0)$. For the simulation displayed in Figure 12, we have chosen the parameters $u = 0.9$, $\rho_c^* = 0.45\rho_{\max}$, and $\Delta\rho^* = 0.1\rho_{\max}$.

F. Heterogeneous and Multi-Lane Traffic

Studies of multi-lane traffic and heterogeneous (multi-userclass) traffic have recently received a considerable amount of interest (Hoogendoorn/Bovy, 1998; Klar/Wegener, 1998a, b; Holland/Woods, 1997; Helbing, 1997d; Helbing/Greiner, 1997). We also mention some earlier proposals (Rørbech, 1976; Michalopoulos/Beskos/Yamauchi, 1984). Most of these models were restricted to the case of small densities or based on various simplifications. Now, the related theoretical and numerical problems are eventually solved.

Here, we shortly present a generalization of the effective one-lane model discussed in Section III B, which explicitly accounts for lane-changes and overtaking maneuvers, as well as for heterogeneous (mixed) traffic with different types a of vehicles (like cars and trucks) that are characterized by different sets of parameter values. As in the the effective one-lane model, we will include effects by vehicular space requirements and velocity correlations at high traffic densities. A more detailled derivation of the model and related simulation results will be presented elsewhere (Shvetsov/Helbing, 1999).

First, let $f_i^a(x,v,t)$ denote the phase-space density of vehicles of type $a \in \{1,\ldots,A\}$ on lane $i \in \{1,\ldots,I\}$, where we count from the slower to the faster lanes. Ramps may be represented by an additional lane $i = 0$. Similar to the continuity equation (16), the phase-space densities obey the equations

$$\frac{\partial f_i^a}{\partial t} + \frac{\partial}{\partial x}(f_i^a v) + \frac{\partial}{\partial v}\left(f_i^a \frac{V_{0i}^a - v}{\tau_i^a}\right) = \left(\frac{df_i^a}{dt}\right)_{\rm int} + \left(\frac{df_i^a}{dt}\right)_{\rm lc}^{\rm int} + \left(\frac{df_i^a}{dt}\right)_{\rm lc}^{\rm spont} . \quad (43)$$

Herein, $(df_i^a/dt)_{\rm int}$ represents deceleration maneuvers in cases, when slower cars cannot be immediately overtaken, $(df_i^a/dt)_{\rm lc}^{\rm int}$ describes interactive lane changes, and $(df_i^a/dt)_{\rm lc}^{\rm spont}$ delineates spontaneous lane changes that are not induced by interactions. Spontaneous lane changes, for example, correspond to switching back to the slow lane after overtaking, in accordance with European traffic regulations. Introducing the abbreviations

$$I_i^{ab}(x,v,t) = \chi_i \int\limits_{v>w} dw\ (v-w) d_{2i}^{ab}(x,v,x+s_i^a,w,t)\,, \quad (44)$$

$$J_i^{ab}(x,v,t) = \chi_i \int\limits_{w>v} dw\ (w-v) d_{2i}^{ab}(x,w,x+s_i^a,v,t) \quad (45)$$

for interaction terms that have been explained in Section III A, we obtain the following expressions: If $p_{i,j}^a$ represents the density-dependent probability of an obstructed vehicle to change from lane i to lane $j \in \{i-1, i+1\}$ and $p_i^a = (p_{i,i-1}^a + p_{i,i+1}^a)$, the interactive braking term reads

$$\left(\frac{\partial f_i^a}{\partial t}\right)_{\rm int} = (1-p_i^a) \sum_b \left[J_i^{ab}(x,v,t) - I_i^{ab}(x,v,t)\right], \quad (46)$$

whereas the lane-changing term due to interactions is

$$\left(\frac{\partial f_i^a}{\partial t}\right)_{\rm lc}^{\rm int} = \sum_b \sum_{j\in\{i-1,i+1\}} \left[p_{j,i}^a I_j^{ab}(x,v,t) - p_{i,j}^a I_i^{ab}(x,v,t)\right], \quad (47)$$

because we have a change in lane instead of a change in velocity. Spontaneous lane changes from lane i to lane $j \in \{i-1, i+1\}$ are proportional to the phase-space densities $f_i^a(x,v,t)$ of vehicles, changes from lane j to i proportional to $f_j^a(x,v,t)$:

$$\left(\frac{\partial f_i^a}{\partial t}\right)_{\rm lc}^{\rm spont} = \sum_{j\in\{i-1,i+1\}} \frac{f_j^a(x,v,t)}{T_{j,i}^a} - \frac{f_i^a(x,v,t)}{T_{i,j}^a}\,. \tag{48}$$

The proportionality factors $1/T_{i,j}^a$ and $1/T_{j,i}^a$, respectively, denote spontanteous lane changing rates. They are characterized by the so-called waiting times $T_{i,j}^a$. A suitable relation is

$$\frac{1}{T_{i,j}^a} = g_{i,j}^a \left(\frac{\rho_i}{\rho_i^{\max}}\right)^{\beta_1} \left(1-\frac{\rho_j}{\rho_j^{\max}}\right)^{\beta_2} \tag{49}$$

with $j \in \{i-1, i+1\}$. This form is rather simple and, at the same time, it is in accordance with empirical data (Sparmann, 1978). The results displayed in this paper are for $\beta_1 = 0$ and $\beta_2 = 8$.

The macroscopic traffic equations for heterogeneous multi-lane traffic can be derived from the above gas-kinetic traffic equations in a similar way as outlined in Section III B. The continuity equations read

$$\frac{\partial \rho_i^a}{\partial t} + \frac{\partial}{\partial x}(\rho_i^a V_i^a) = \sum_{b=1}^{A} \sum_{j\in\{i-1,i+1\}} \left[\rho_j^a \rho_j'^b p_{j,i}^a \chi(\rho_j') A(\Delta V_j^{ab}) - \rho_i^a \rho_i'^b p_{i,j}^a \chi(\rho_i') A(\Delta V_i^{ab})\right] \tag{50}$$

$$+ \sum_{j\in\{i-1,i+1\}} \left(\frac{\rho_j^a}{T_{j,i}^a} - \frac{\rho_i^a}{T_{i,j}^a}\right). \tag{51}$$

Compared to equation (1), they contain additional terms due to interactive and spontaneous lane changes. The expressions

$$\Delta V_i^{ab} = \frac{V_i^a - V_i'^b}{\sqrt{S_i^{ab}}} \tag{52}$$

with

$$S_i^{ab} = \theta_i^a - 2r_i^{ab}\sqrt{\theta_i^a \theta_i'^b} + \theta_i'^b \tag{53}$$

denote lane-specific, effective dimensionless velocity differences, which depend on the interacting vehicle types. Furthermore, we have used another Boltzmann factor

$$A(\Delta V_i^{ab}) = \sqrt{S_i^{ab}}\left[N(\Delta V_i^{ab}) + \Delta V_i^{ab} E(\Delta V_i^{ab})\right]. \tag{54}$$

The equation for the traffic flow of vehicles of type a on lane i is

$$\begin{aligned}\frac{\partial}{\partial t}(\rho_i^a V_i^a) + \frac{\partial}{\partial x}\left\{\rho_i^a[(V_i^a)^2 + \theta_i^a]\right\} &= \frac{\rho_i^a(V_{0i}^a - V_i^a)}{\tau_i^a} - (1-p_i^a)\sum_b \rho_i^a \rho_i'^b \chi(\rho_i') B(\Delta V_i^{ab}) \\ &+ \sum_j \sum_b \left[\rho_j^a \rho_j'^b p_{j,i}^a \chi(\rho_j') C(\Delta V_j^{ab}) - \rho_i^a \rho_i'^b p_{i,j}^a \chi(\rho_i') C(\Delta V_i^{ab})\right] \\ &+ \sum_j \left(\frac{\rho_j^a V_j^a}{T_{j,i}^a} - \frac{\rho_i^a V_i^a}{T_{i,j}^a}\right),\end{aligned} \tag{55}$$

with the Boltzmann factors

$$B(\Delta V_i^{ab}) = S_i^{ab}\left\{\Delta V_i^{ab} N(\Delta V_i^{ab}) + [1 + (\Delta V_i^{ab})^2] E(\Delta V_i^{ab})\right\} \tag{56}$$

and

$$C(\Delta V_i^{ab}) = S_i^{ab}\left[\frac{V_i^a}{\sqrt{S_i^{ab}}} N(\Delta V_i^{ab}) + \left(\frac{\theta_i^a - r_i^{ab}\sqrt{\theta_i^a \theta_i'^b}}{S_i^{ab}} + \frac{V_i^a}{\sqrt{S_i^{ab}}}\,\Delta V_i^{ab}\right) E(\Delta V_i^{ab})\right]. \tag{57}$$

The last two lines of equation (55) originate also from interactive and spontaneous lane changes.

The above model has been successfully calibrated to empirical traffic data of the Dutch motorway A9. Good results were obtained for the parameters displayed in Table II and the relations

$$\chi_i(\rho_i) = 1 + \frac{V_{0i} T_i^2}{\tau_i \alpha_i (\rho_i^{\max})} \frac{\rho_i}{(1-\rho_i/\rho_i^{\max})^2}\,, \tag{58}$$

$$p_i^a(\rho_i) = \frac{\exp\left(-p_{0i}^a \rho_i/\rho_i^{\max}\right)}{\chi_i(\rho_i)}\,. \tag{59}$$

Here, variables without an index for the specific vehicle type a represent weighted averages of the variables belonging to the different vehicle types in lane i, for example,

$$T_i = \sum_{a=1}^{A} \frac{\rho_i^a}{\rho_i} T_i^a\,. \tag{60}$$

Note that, at low densities, lane changes correspond mainly to interactive lane changes from the right to the left lane and to spontaneous lane changes from the left to the right lane (see Figure 13). This is plausible for European traffic, where vehicles tend to interactively overtake on the fast lane and spontaneously switch back to the slow lane. In order to describe the empirically observed density-dependence of the total lane changing rates, the lane occupancies [Figure 14(a)], and the density difference among lanes [Figure 14(b)], correctly, it turned out that one needs to consider both, spontaneous *and* interactive lane changes.

Apart from the density-dependence of the lane-changing rates (Sparmann, 1978) and the density difference among lanes, the resulting model fits the observed variance-density relations, the velocity-density relations, and the occupancies of the different lanes very well. Our model also allows to reproduce the traffic dynamics at bottlenecks (Shvetsov/Helbing, 1999) and the tendency of velocity synchronization among lanes. Here, we display simulation results that show the spreading of a small disturbance in traffic flow from one lane to another (Figure 15). The evolving dynamical traffic patterns are very similar, because of lane-changes that compensate for developing disequilibria. Nevertheless, the dynamics in both lanes is not identical due to the significantly different parameter sets for each lane (see Table II). In addition, we have compared the average dynamics of both lanes with the dynamics of the effective one-lane model with intermediate parameter values. We find a qualitative agreement of the main features of the dynamics, but some details are different due to the non-linearity of the equations (Figure 16). This indicates that effective one-lane models can achieve a satisfactory, but not perfect representation of multi-lane dynamics.

Our present investigations focus on the empirical evaluation of velocity correlations between interacting vehicles and on the calibration of the model to a mixture of vehicle types like cars and trucks, both of which are difficult tasks. We expect that this will allow us to describe the effects of heterogeneous traffic which were recently found in microscopic models (Helbing/Huberman, 1998; Helbing/Schreckenberg, 1999).

IV. SUMMARY AND OUTLOOK

We have proposed an improved gas-kinetic traffic model and its associated macroscopic traffic equations, which were derived from a microscopic model of vehicle dynamics. The model differs from others mainly by its non-local interaction term that takes into account space requirements of vehicles and the correlations of successive vehicle velocities. It reflects the anticipation behavior of drivers and is responsible for a smoothing effect that acts only in backward direction. As a consequence, the model behaves very realistically, even in situations of artificially produced shock

fronts. Moreover, it allows a robust and efficient simulation of several thousand freeway kilometers in real-time.

According to our model, at intermediate densities homogeneous traffic behaves unstable with respect to perturbations, leading to non-linear states like localized clusters, stop-and-go waves, or dipole-like structures, while homogeneous traffic flow is stable for high and low densities. In addition, our model reproduces the observation that the outflow $Q_{\rm out}$ from traffic jams and their dissolution velocity C are independent from the spatially averaged density and from the particular initial conditions, because the outflow region in front of congested traffic is nearly independent of how it was formed.

Furthermore, our model allows to simulate "synchronized" congested traffic, which turned out to be the most frequent form of congested traffic (Kerner/Rehborn, 1997). It mainly occurs close to on-ramps. By variation of the on-ramp flow, we could reproduce all known transitions between free traffic, synchronized traffic, and stop-and-go traffic. For the macroscopic simulation of traffic including on- and off-ramps, we have developed a flexible program package called MASTER (which stands for Macroscopic Simulation of Traffic to Enable Road Predictions). An extension of the simulation model to the case of heterogeneous multi-lane traffic is also available. The applied numerical solution methods are described in another paper (Helbing/Treiber, 1998d).

Acknowledgments

The authors want to thank for financial support by the BMBF (research project SANDY, grant No. 13N7092) and by the DFG (Heisenberg scholarship He 2789/1-1). They are also grateful to Henk Taale and the Dutch *Ministry of Transport, Public Works and Water Management* for supplying the freeway data.

---

[1] Andrews, F. C. (1970) A statistical theory of traffic flow on highways—II. Three-car interactions and the onset of queuing. *Transportation Research* **4**, 367–377.

[2] Andrews, F. C. (1973a) A statistical theory of traffic flow on highways—III. Distributions of desired speeds. *Transportation Research* **7**, 223–232.

[3] Andrews, F. C. (1973b) A statistical theory of traffic flow on highways—IV. Semi-empirical steady state theory. *Transportation Research* **7**, 233–241.

[4] Bando, M., Hasebe, K., Nakanishi, K., Nakayama, A., Shibata, A., and Sugiyama, Y. (1995) Phenomenological study of dynamical model of traffic flow *Journal de Physique I France* **5**, 1389–1399.

[5] Beylich, A. E. (1979) Elements of a kinetic theory of traffic flow. *Rarefied Gas Dynamics, Vol. 1*, ed. R. Campargue, pp. 129–138. Commissariat a l'Energie Atomique, Paris.

[6] Beylich, A. E. (1981) Zur Entwicklung einer kinetischen Theorie des Verkehrsflusses. *Neue Wege in der Mechanik*, eds. G. Adomeit and H.-J. Frieske, pp. 171–175. VDI-Verlag, Düsseldorf.

[7] Bovy, P. H. L., ed. (1998) *Motorway Traffic Flow Analysis. New Methodologies and Recent Empirical Findings*. Delft University Press, Delft.

[8] Cremer, M. (1979) *Der Verkehrsfluß auf Schnellstraßen*. Springer, Berlin.

[9] Cross, M. C. and Hohenberg, P. C. (1993) Pattern formation outside of equilibrium. *Reviews of Modern Physics* **65**, 851–1112 (1993).

[10] Daganzo, C. F. (1994) The cell transmission model: A dynamic representation of highway traffic consistent with the hydrodynamic theory. *Transportation Research B* **28**, 269–287.

[11] Daganzo, C. F. (1995a) The cell transmission model, Part II: Network traffic. *Transportation Research B* **29**, 79–93.

[12] Daganzo, C. F. (1995b) Requiem for second-order fluid approximations of traffic flow. *Transportation Research B* **29**, 277–286.
[13] Daganzo, C. F. (1997) A continuum theory of traffic dynamics for freeways with special lanes. *Transportation Research B* **31**, 83–102.
[14] Daganzo, C. F. (1998) The nature of the freeway gridlock and how to prevent it. *Transportation Research B*, submitted.
[15] Daganzo, C. F., Cassidy, M. J., and Bertini, R. L. (1998) Possible explanations of phase transitions in highway traffic. *Transportation Research B*, submitted.
[16] Daganzo, C. F., Lin, W.-H., and Del Castillo, J. M. (1997) A simple physical principle for the simulation of freeways with special lanes and priority vehicles. *Transportation Research B* **31**, 103–125.
[17] Gerlough, D. L. and Huber, M. J. (1975) *Special Report 165: Traffic Flow Theory.* Transportation Research Board, Washington, D.C.
[18] Helbing, D. (1996a) Gas-kinetic derivation of Navier-Stokes-like traffic equations. *Physical Review E* **53**, 2366–2381.
[19] Helbing, D. (1996b) Derivation and empirical validation of a refined traffic flow model. *Physica A* **233**, 253–282.
[20] Helbing, D. (1997a) *Verkehrsdynamik.* Springer, Berlin.
[21] Helbing, D. (1997b) Empirical traffic data and their implications for traffic modeling. *Physical Review E* **55**, R25-R28.
[22] Helbing, D. (1997c) Fundamentals of traffic flow. *Physical Review E* **55**, 3735–3738.
[23] Helbing, D. (1997d) Modeling multi-lane traffic flow with queuing effects. *Physica A* **242**, 175–194 (1997).
[24] Helbing, D. (1998) From microscopic to macroscopic traffic models. *A Perspective Look at Nonlinear Media. From Physics to Biology and Social Sciences*, eds. J. Parisi, S. C. Müller, and W. Zimmermann, pp. 122–139. Springer, Berlin.
[25] Helbing, D. and Greiner, A. (1997) Modeling and simulation of multilane traffic flow. *Physical Review E* **55**, 5498–5507.
[26] Helbing, D., Hennecke, A., and Treiber, M. (1998) Phase diagram of traffic states in the presence of inhomogeneities. Submitted to *Physical Review Letters.*
[27] Helbing, D. and Huberman, B. A. (1998) Coherent moving states in highway traffic. *Nature* **396**, 738–740.
[28] Helbing, D. and Schreckenberg, M. (1999) Cellular automata simulating experimental properties of traffic flow. *Physical Review E*, in print.
[29] Helbing, D. and Treiber, M. (1998a) Enskog equations for traffic flow evaluated up to Navier-Stokes order. *Granular Matter* **1**, 21–31.
[30] Helbing, D. and Treiber, M. (1998b) Gas-kinetic-based traffic model explaining observed hysteretic phase transition. *Physical Review Letters* **81**, 3042-3045.
[31] Helbing, D. and Treiber, M. (1998c) Jams, waves, and clusters. *Science* **282**, 2001–2003.
[32] Helbing, D. and Treiber, M. (1998d) Numerical simulation of macroscopic traffic equations. *Computing in Science and Engineering*, in print.
[33] Hilliges, M. and Weidlich, W. (1995) A phenomenological model for dynamic traffic flow in networks. *Transportation Research B* **29**, 407–431.
[34] Holland, E. N. and Woods, A. W. (1997) A continuum model for the dispersion of traffic on two-lane roads. *Transportation Research B* **31**, 473–485.
[35] Hoogendoorn, S. and Bovy, P. H. L. (1998) A macroscopic multi-lane multi-class traffic flow model. Paper submitted for presentation and publication to the 79th TRB Annual Meeting 1999 in Washington.
[36] Islam, M. N. and Consul, P. C. (1991) The Consul distribution as a bunching model in traffic flow. *Transporation Research B* **25**, 365–372.
[37] Kerner, B. S. (1997) Experimental characteristics of traffic flow for evaluation of traffic modelling. *Transportation Systems*, Vol. II, eds. M. Papageorgiou and A. Pouliezos, pp. 793–798. International Federation of Automatic Control, Chania, Greece.
[38] Kerner, B. S. (1998) Experimental features of self-organization in traffic flow. *Physical Review Letters* **81**, 3797–3800.
[39] Kerner, B. S. and Konhäuser, P. (1993) Cluster effect in initially homogeneous traffic flow. *Physical Review E* **48**, R2335–R2338.
[40] Kerner, B. S. and Konhäuser, P. (1994) Structure and parameters of clusters in traffic flow. *Physical Review E* **50**, 54–83.
[41] Kerner, B. S., Konhäuser, P., and Schilke, M. (1995) Deterministic spontaneous ap-

pearance of traffic jams in slightly inhomogeneous traffic flow. *Physical Review E* **51**, R6243–R6246.

[42] Kerner, B. S., Konhäuser, P., and Schilke, M. (1996) "Dipole-layer" effect in dense traffic flow. *Physics Letters A* **215**, 45–56.

[43] Kerner, B. S. and Rehborn, H. (1996a) Experimental features and characteristics of traffic jams. *Physical Review E* **53**, R1297–R1300.

[44] Kerner, B. S. and Rehborn, H. (1996b) Experimental properties of complexity in traffic flow. *Physical Review E* **53**, R4275–R4278.

[45] Kerner, B. S. and Rehborn, H. (1997) Experimental properties of phase transitions in traffic flow. *Physical Review Letters* **49**, 4030–4033.

[46] Klar, A. and Wegener, R. (1997) Enskog-like kinetic models for vehicular traffic. *Journal of Statistical Physics* **87**, 91–114.

[47] Klar, A. and Wegener, R. (1998a) A hierarchy of models for multilane traffic I: Modeling. To appear in *SIAM Journal of Applied Mathematics*.

[48] Klar, A. and Wegener, R. (1998b) A hierarchy of models for multilane traffic II: Numerical investigations. To appear in *SIAM Journal of Applied Mathematics*.

[49] Kühne, R. D. (1984) Macroscopic freeway model for dense traffic—Stop-start waves and incident detection. *Proceedings of the 9th International Symposium on Transportation and Traffic Theory*, eds. I. Volmuller and R. Hamerslag, pp. 21–42. VNU Science Press, Utrecht, The Netherlands.

[50] Kühne, R. D. (1987) Freeway speed distribution and acceleration noise—Calculations from a stochastic continuum theory and comparison with measurements. *Proceedings of the 10th International Symposium on Transportation and Traffic Theory*, eds. N. H. Gartner and N. H. M. Wilson, pp. 119–137. Elsevier, New York.

[51] Lampis, M. (1978) On the kinetic theory of traffic flow in the case of a nonnegligible number of queueing vehicles. *Transportation Science* **12**, 16–28.

[52] Lebacque, J. P. (1997) A finite acceleration scheme for first order macroscopic traffic flow models *Transportation Systems*, Vol. II, eds. M. Papageorigiou and A. Pouliezos, pp. 815–820. International Federation of Automatic Control, Chania, Greece.

[53] Leutzbach, W. (1988) *Introduction to the Theory of Traffic Flow*. Springer, Berlin.

[54] Lighthill, M. J. and Whitham, G. B. (1955) On kinematic waves: II. A theory of traffic on long crowded roads. *Proceedings of the Royal Society A* **229**, 317–345.

[55] May, A. D. (1990) *Traffic Flow Fundamentals*. Prentice Hall, Englewood Cliffs, NJ.

[56] Michalopoulos, P. G., Beskos, D. E., and Yamauchi, Y. (1984) Multilane traffic flow dynamics: Some macroscopic considerations. *Transportation Research B* **18**, 377–395.

[57] Nelson, P. (1995) A kinetic model of vehicular traffic and its associated bimodal equilibrium solutions. *Transport Theory and Statistical Physics* **24**, 383–409.

[58] Newell, G. F. (1993a) A simplified theory of kinematic waves in highway traffic, Part I: General theory. *Transportation Research B* **27**, 281–287.

[59] Newell, G. F. (1993b) A simplified theory of kinematic waves in highway traffic, Part II: Queueing at freeway bottlenecks. *Transportation Research B* **27**, 289–303.

[60] Newell, G. F. (1993c) A simplified theory of kinematic waves in highway traffic, Part III: Multi-destination flows. *Transportation Research B* **27**, 305–313.

[61] Pampel, F. (1955) *Ein Beitrag zur Berechnung der Leistungsfähigkeit von Straßen*. Kirschbaum, Bielefeld.

[62] Papageorgiou, M. (1983) *Applications of Automatic Control Concepts to Traffic Flow Modeling and Control*. Springer, Berlin.

[63] Paveri-Fontana, S. L. (1975) On Boltzmann-like treatments for traffic flow. A critical review of the basic model and an alternative proposal for dilute traffic analysis. *Transportation Research* **9**, 225–235.

[64] Payne, H. J. (1971) Models of freeway traffic and control. *Mathematical Models of Public Systems*, Vol. 1, ed. G. A. Bekey, pp. 51–61. Simulation Council, La Jolla, CA.

[65] Phillips, W. F. (1979) A kinetic model for traffic flow with continuum implications. *Transportation Planning and Technology* **5**, 131–138.

[66] Poethke, H. J. (1982) *Ein Vierphasenmodell des Verkehrsflusses auf Autobahnen*. PhD thesis, Fakultät für Maschinenwesen, RWTH Aachen.

[67] Prigogine, I. and Herman, R. (1971) *Kinetic Theory of Vehicular Traffic*. Elsevier, New York.

[68] Raub, R. A. and Pfefer (1998) Vehicular flow past incidents involving lane blockage on urban roads: A preliminary exploration *77th TRB Annual Meeting*, manuscript no. 004.

Transportation Research Board, Washington, D.C.
[69] Richards, P. I. (1956) Shock waves on the highway. *Operations Research* **4**, 42–51.
[70] Rørbech, J. (1976) Multilane traffic flow process: Evaluation of queuing and lane-changing patterns. *Transportation Research Record* **596**, 22–29.
[71] Schreckenberg, M. and Wolf, D. E., eds. (1998) *Traffic and Granular Flow '97*. Springer, Singapore.
[72] Shvetsov, V. and Helbing, D. (1999) Macroscopic dynamics of multi-lane traffic. *Physical Review E*, submitted.
[73] Sparmann, U., ed. (1978) *Spurwechselvorgänge auf zweispurigen BAB-Richtungsfahrbahnen*. Vol. 263 of *Forschung Straßenbau und Straßenverkehrstechnik*. Bundesministerium für Verkehr, Abt. Straßenbau, Bonn-Bad Godesberg.
[74] Treiber, M. and Helbing, D. (1999a) Macroscopic simulation of widely scattered traffic states. *J. Phys. A: Math. Gen.* **32**, L17-L23.
[75] Treiber, M. and Helbing, D. (1999b) Explanation of observed features of self-organization in traffic flow. Submitted to *Physical Review Letters*.
[76] Treiber, M., Hennecke, A., and Helbing, D. (1999) Derivation, properties, and simulation of a gas-kinetic-based, non-local traffic model. *Physical Review E* **59**, 239–253.
[77] Wagner, C., *et al.* (1996) Second order continuum traffic flow model. *Physical Review E* **54**, 5073–5085.
[78] Whitham, G. B. (1974) *Linear and Nonlinear Waves*. Wiley, New York.

Parameter	Symbol	Typical Value
Desired Velocity	V_0	110 km/h
Maximum Density	$\rho_{\max}$	160 vehicles/km/lane
Acceleration Relaxation Time	τ	35 s
Safe Time Headway	T	1.8 s
Anticipation Factor	γ	1.2

TABLE I. Typical values of model parameters for traffic on the Dutch freeway A9.

Parameter	Symbol	Right Lane	Left Lane
Desired Velocity	V_0	105 km/h	123 km/h
Maximum Density	$\rho^{\max}$	150 vehicles/km	150 vehicles/km
Acceleration Relaxation Time	τ	35 s	35 s
Safe Time Headway	T	1.7 s	1.2 s
Anticipation Factor	γ	1.2	1.2
Coefficients for Variance Approximation	α_0	0.007	0.0065
	$\Delta\alpha$	0.03	0.036
	$\rho_{\rm c}$	0.275 $\rho^{\max}$	0.305 $\rho^{\max}$
	$\Delta\rho$	0.03 $\rho^{\max}$	0.025 $\rho^{\max}$
Coefficient for Overtaking Probability	p_0	17.0	12.5
Coefficient for Spontaneous Lane-Changing	$g_{i,3-i}$	75	28

TABLE II. The estimated parameter values for the two-lane, single vehicle-class model, calibrated to traffic data from the Dutch motorway A9.

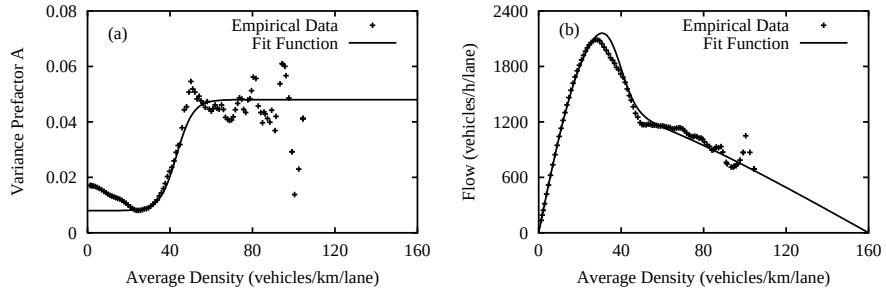

FIG. 1. Comparison of (a) the density-dependent relative variance Θ in units of the squared average velocity, and (b) the equilibrium flow-density relation (38) of our gas-kinetic-based traffic model (solid lines) with empirical data (crosses). The empirical data were obtained from single-vehicle data of the Dutch motorway A9 (where a speed limit of 120 km/h applies), by averaging over one-minute intervals. Note that both, the variance-density relation and the velocity-density relation in equilibrium, are fitted by a single, density-dependent function $\alpha(\rho)$. It turns out that the deviation of the variance-density relation from the empirical data at small densities is not of great importance for the dynamics of the traffic model. It can, however, be accounted for by the function $W(\rho)$, see formulas (30) and (31).

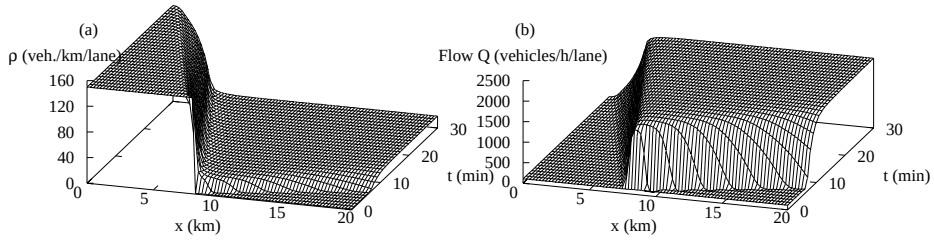

FIG. 2. Simulation of a downstream front with a jam density of 140 vehicles/km/lane. Shown is the spatio-temporal development (a) of the density $\rho(x,t)$, and (b) the flow $Q(x,t) = \rho(x,t)V(x,t)$. Free boundary conditions were used on both sides.

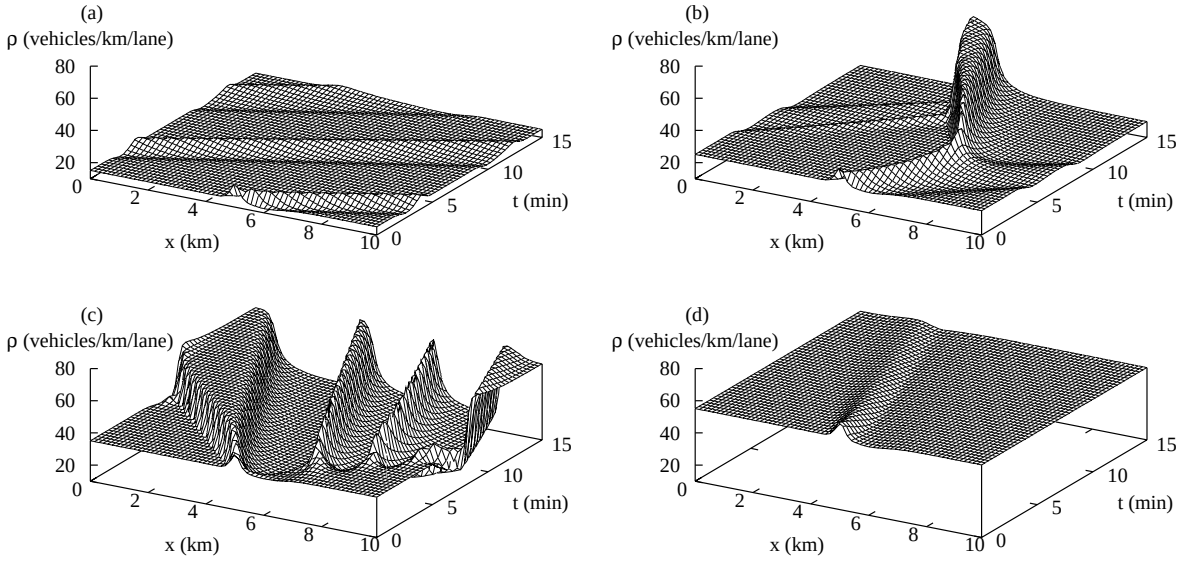

FIG. 3. Spatio-temporal evolution of the traffic density $\rho(x,t)$ on a uni-directional ring of circumference 10 km, starting with initially homogeneous traffic to which a localized perturbation of amplitude 10 vehicles/km/lane is added. (a) is for free and stable traffic at an average density 15 vehicles/km/lane, (b) is for metastable traffic at 25 vehicles/km/lane, (c) is for unstable traffic at 35 vehicles/km/lane, and (d) is for stable congested traffic at 55 vehicles/km/lane). The chosen model parameters are displayed in Table I.

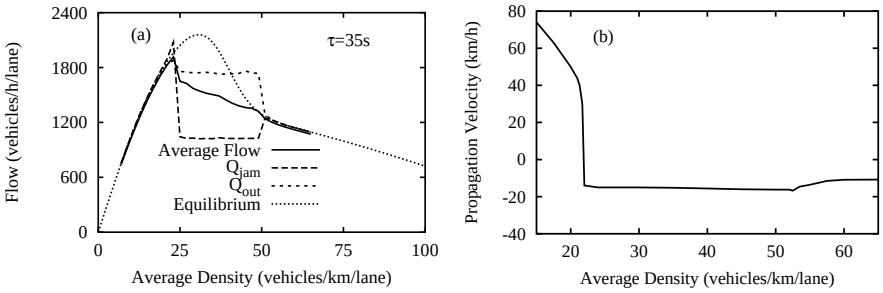

FIG. 4. (a) Characteristic flows resulting in fully developed stop-and-go traffic on a circular road, as a function of the spatially averaged density. Depicted are the flows $Q_{\rm jam}$ in the jammed regions (– –), the outflows $Q_{\rm out}$ from jams (- - -), and the average flows (—). For comparison, the equilibrium flow $Q_{\rm e} = \rho V_{\rm e}$ with $V_{\rm e}$ from equation (36) is also shown ($\cdots$). Notice that, in the unstable range, the average *dynamic* flow is lower than the equilibrium flow. (b) Propagation velocity of density clusters as a function of average density. We started our simulations with an initial perturbation of amplitude 10 vehicles/km/lane and measured the group velocity after a sufficiently long transient time. The propagation velocity at low densities is positive, but slower than the average vehicle velocity. In the instability region, the negative propagation velocity of fully developed traffic jams (i.e. their dissolution velocity) is independent of the initial density, and its magnitude is in agreement with empirical data. Notice that the dissolution velocity C of jam fronts corresponds to the slope of the average flow depicted in (a).

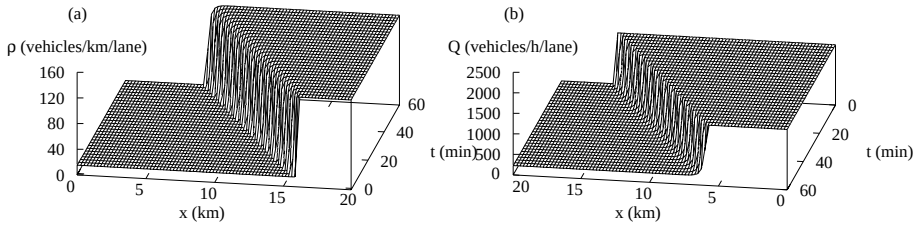

FIG. 5. Simulation of an upstream front with initial densities of $\rho_1 = 15$ vehicles/km/lane and $\rho_2 = 140$ vehicles/km/lane. Shown is the evolution of (a) the density $\rho(x,t)$, and (b) the flow $Q(x,t) = \rho(x,t)V(x,t)$. Note that, in contrast to other macroscopic traffic models (Daganzo, 1995b), the simulations do *not* produce densities above $\rho_{\max}$ or negative flows. In (b), the direction of the space and time axes is reversed for illustrative reasons.

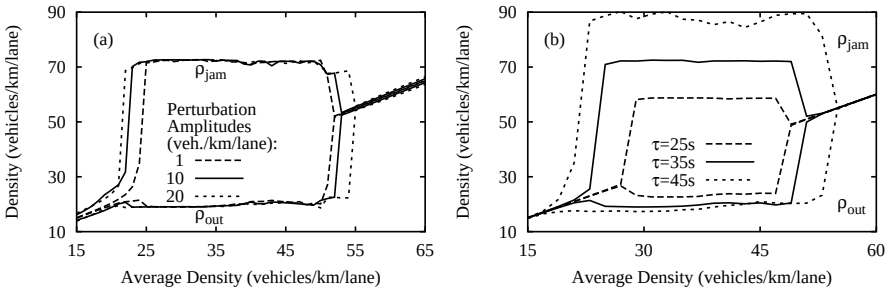

FIG. 6. Stability diagram for a localized perturbation of homogeneous traffic on a ring of circumference 10 km. Both diagrams show the developing maximum and minimum densities $\rho_{\rm jam}$ and $\rho_{\rm out}$, as a function of the spatially averaged density, measured after a dynamical equilibrium was reached. The unstable traffic regime corresponds to the density range where the jam amplitude ($\rho_{\rm jam} - \rho_{\rm out}$) is large (rectangle-like shaped regions). Diagram (a) shows the dependence of the stability diagram on the perturbation amplitude $\Delta\rho$. One can clearly see two density ranges $[\rho_{\rm c1}, \rho_{\rm c2}]$ with $\rho_{\rm c1} = 21$ vehicles/km/lane and $\rho_{\rm c2} = 24$ vehicles/km/lane, and $[\rho_{\rm c3}, \rho_{\rm c4}]$ with $\rho_{\rm c3} = 51$ vehicles/km/lane and $\rho_{\rm c4} = 55$ vehicles/km/lane, where traffic is non-linearly stable, i.e., stable for small perturbations, but unstable for large perturbations. In the range $[\rho_{\rm c2}, \rho_{\rm c3}]$, homogeneous traffic is unstable for arbitrary perturbation amplitudes. Diagram (b) shows the stability diagram for various relaxation times τ and a perturbation amplitude of $\Delta\rho = 1$ vehicle/km/lane.

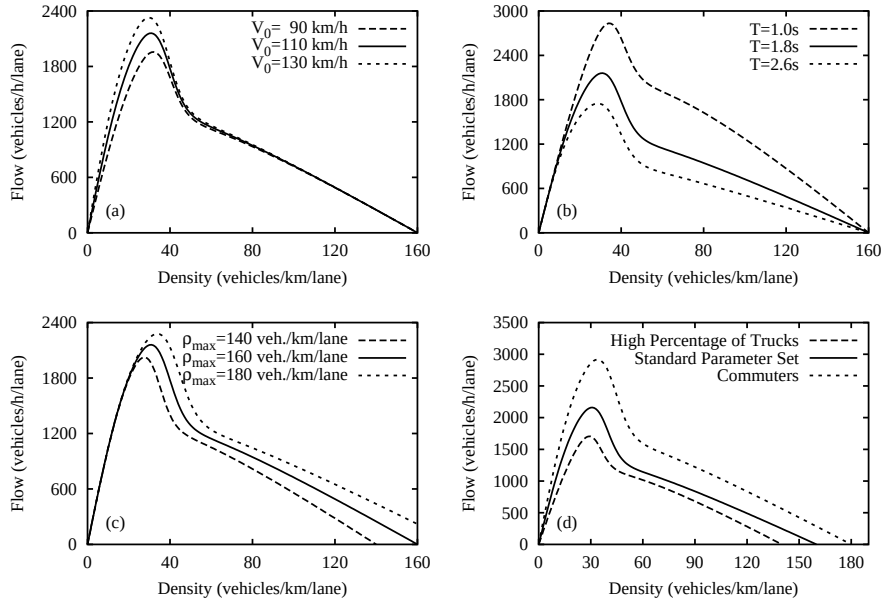

FIG. 7. Equilibrium flow-density relations of the non-local, gas-kinetic-based traffic model. The diagrams (a) through (c) show the variation with the model parameters V_0, T, and $\rho_{\max}$. Notice that a reasonable speed limit almost does not affect the flow in the congested regime. Diagram (d) shows parameter combinations typical for an increased percentage of trucks ($V_0 = 80\,\mathrm{km/h}$, $T = 1.8\,\mathrm{s}$, $\rho_{\max} = 140\,\mathrm{vehicles/km/lane}$), or a decreased percentage as expected in commuter traffic ($V_0 = 140\,\mathrm{km/h}$, $T = 1.4\,\mathrm{s}$, $\rho_{\max} = 180\,\mathrm{vehicles/km/lane}$). In each diagram, the solid lines correspond to the standard parameter set displayed in Table I.

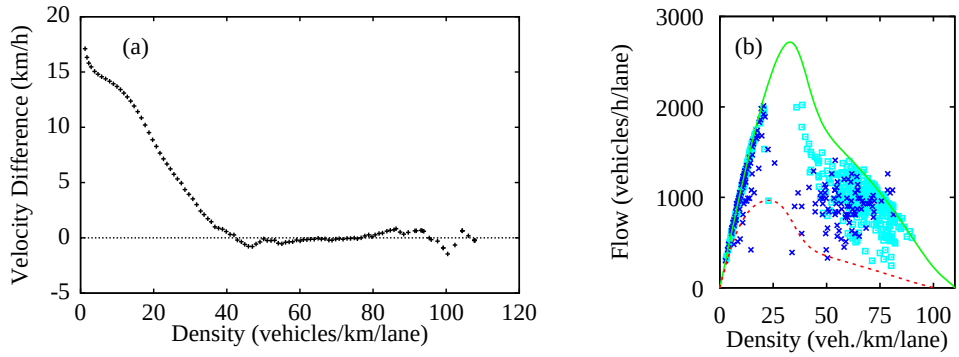

FIG. 8. (a) Difference between the average velocity $V_2(\rho)$ in the left lane and $V_1(\rho)$ in the right lane as a function of the lane-averaged vehicle density ρ. The data points correspond to averages of one-minute data that were evaluated from single-vehicle data of the Dutch freeway A9. (b) The displayed points in flow-density space correspond to lane-averaged one-minute data (dark crosses) and related simulation results (grey boxes) at the location of an on-ramp. The simulations manage to reproduce both, the quasi-linear flow-density relation at small densities and the scattering over a two-dimensional region at high densities. They are based on the assumption that, in an effective model of mixed traffic, the time-dependent parameters $X(t)$ are given by a linear interpolation $X(t) = \{p_{\rm truck}(t)X_{\rm truck} + [1-p_{\rm truck}(t)]X_{\rm car}\}$ between the parameters $X_{\rm car}$ of cars and $X_{\rm truck}$ of trucks, where $p_{\rm truck}(t)$ denotes the time-dependent truck fraction passing the cross section. By lines, we have displayed the assumed equilibrium flow-density relations for traffic consisting of 100% cars (—), and of 100% trucks (- - -).

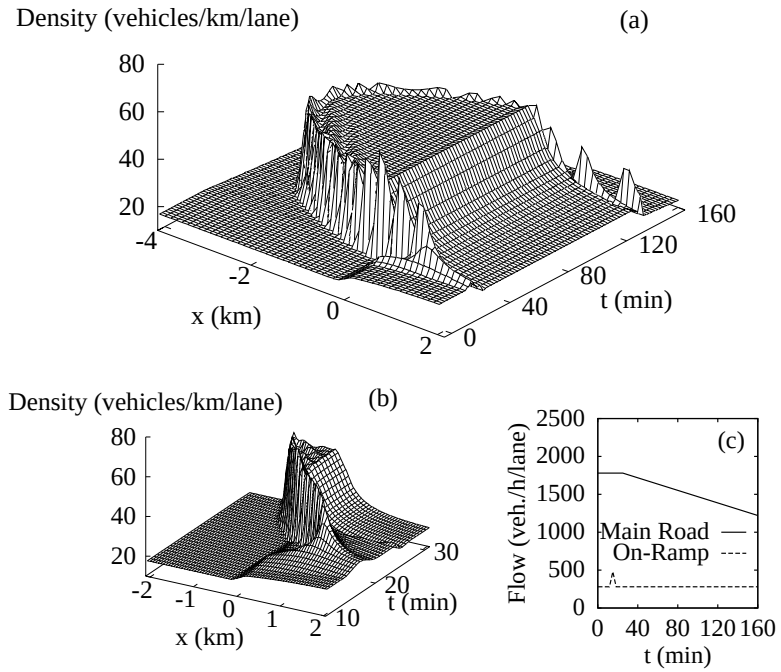

FIG. 9. Spatio-temporal evolution of the lane-averaged density after a small peak of inflow from the on-ramp. The on-ramp merges with the main road at $x = 0\,\mathrm{km}$ with a merging length of $L = 300\,\mathrm{m}$. Traffic flows from left to right. In (a), the parabolically shaped region of high density corresponds to "synchronized" congested traffic. Plot (b) shows the formation of this state in more detail. The time-dependent inflows Q_{main} at the upstream boundary and Q_{rmp}/n at the on-ramp are displayed in (c).

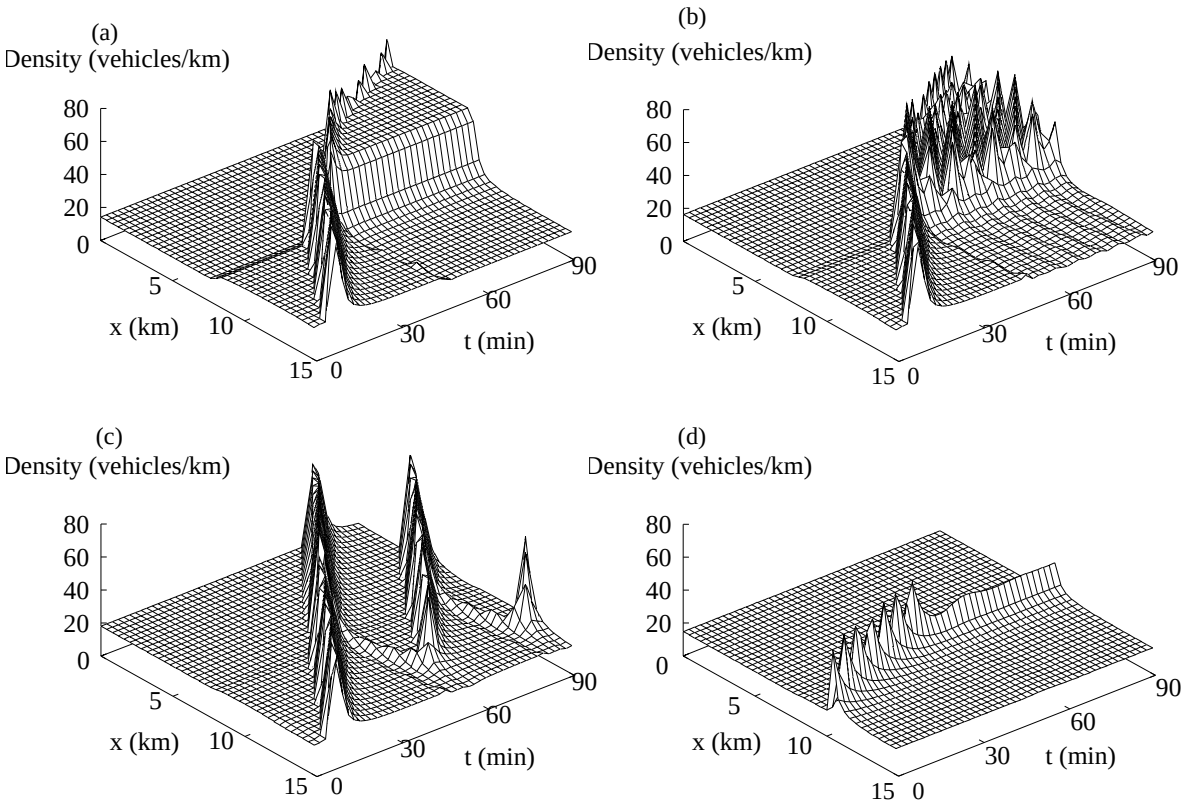

FIG. 10. Spatio-temporal dynamics of typical representatives of congested states which are triggered at on on-ramp by a fully developed perturbation travelling upstream. The middle of the on-ramp is located at $x = 8.0$ km. The respective states are (a) homogeneous congested traffic (HCT) for $Q_{\rm main} = 1350$ vehicles/h/lane and $Q_{\rm rmp}/n = 400$ vehicles/h, (b) oscillatory congested traffic (OCT) for $Q_{\rm main} = 1540$ vehicles/h/lane and $Q_{\rm rmp}/n = 170$ vehicles/h, (c) triggered stop-and-go traffic (TSG) for $Q_{\rm main} = 1660$ vehicles/h/lane and $Q_{\rm rmp}/n = 75$ vehicles/h, and (d) a pinned localized cluster (PLC) for $Q_{\rm main} = 1450$ vehicles/h/lane and $Q_{\rm rmp}/n = 60$ vehicles/h. The other model parameters used in the above simulations are $V_0 = 110$ km/h, $\rho_{\rm max} = 140$ Fz/km, $\tau = 40$ s, $T = 1.7$ s, $\gamma = 1.2$, $\alpha_0 = 0.008$, $\Delta\alpha = 0.02$, $\rho_c = 0.27\rho_{\rm max}$, $\delta\rho = 0.1\rho_{\rm max}$, and $L = 400$ m. They can be considered as typical for German freeways.

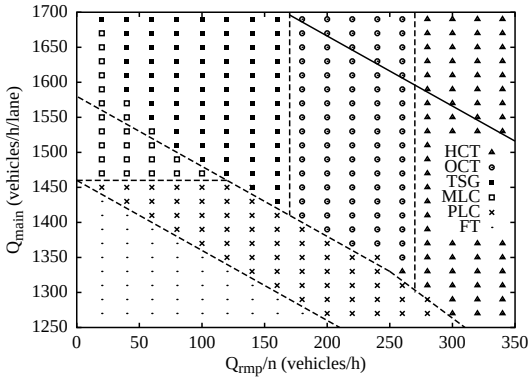

FIG. 11. Phase diagram of the traffic states forming in the vicinity of an on-ramp as a function of the inflows Q_{main} and Q_{rmp}/n per freeway lane on the main road and the on-ramp for the parameters used in Figure 10. The different states are classified at $t = 90$ min, i.e., after a sufficiently long transient period. Displayed are homogeneous congested traffic (HCT), oscillatory congested traffic (OCT), triggered stop-and-go traffic (TSG), moving localized clusters (MLC), pinned localized clusters (PLC), and free traffic (FT). The states are triggered by a fully developed localized cluster travelling upstream and passing the ramp, compare Figure 10. Dashed lines indicate the theoretical phase boundaries. The solid line represents the condition $Q_{\mathrm{main}} + Q_{\mathrm{rmp}}/n = Q_{\mathrm{max}}$ that separates the region, in which a breakdown of traffic flow is caused by exceeding the theoretically possible freeway capacity Q_{max} (upper left corner). Note that all congested traffic states below this line are caused by perturbations and, therefore, avoidable by technical control measures.

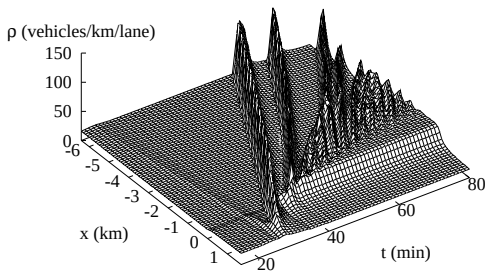

FIG. 12. Spatiotemporal density plot illustrating the breakdown to "synchronized" congested traffic (smooth region of high density) near a bottleneck, and showing stop-and-go waves emanating from this region. The assumed bottleneck of traffic flow comes from an on-ramp of length 200 m with an inflow of 220 vehicles per hour and freeway lane. The inflow to the main road is 1570 vehicles per hour and lane, and the breakdown of traffic flow is triggered by a short perturbation of the inflow with a flow peak of 125 vehicles per hour and lane. The assumed model parameters are $V_0 = 120$ km/h, $T = 1.5$ s, $\tau = 30$ s, $\rho_{\max} = 120$ vehicles/km/lane, and $\gamma = 1.2$, while the parameters for the variance prefactor are $\alpha_0 = 0.008$, $\Delta\alpha = 0.02$, $\rho_c = 0.27\rho_{\max}$, and $\Delta\rho = 0.1\rho_{\max}$.

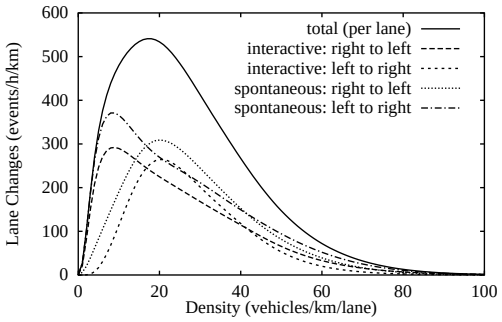

FIG. 13. Equilibrium lane-changing rates according to our multi-lane model as a function of the lane-averaged density. Note that, at small densities, we have more interactive lane changes from the right to the left lane ("overtaking maneuvers") and more spontaneous lane changes from the left to the right lane, as expected for European traffic.

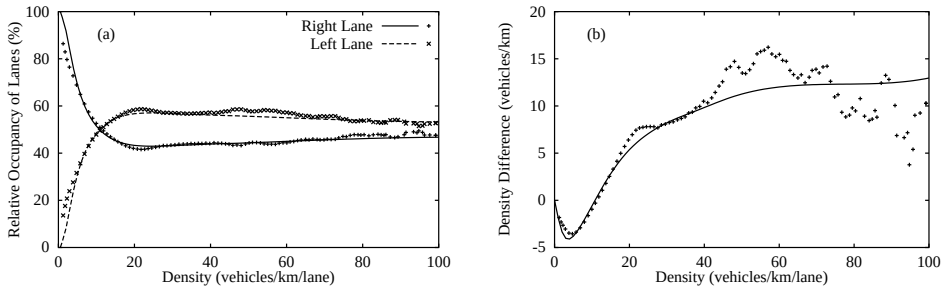

FIG. 14. (a) Fit of the lane occupancy on the Dutch highway A9, i.e. of the percentage of the vehicle density in a lane compared to the total density in all lanes. Symbols correspond to empirical data, lines to the results of our multi-lane model. The preference for the right lane at small densities comes from the European traffic regulations. (b) Theoretical (—) and empirical (+) difference of the densities in the left and the right lane as a function of the lane-averaged density.

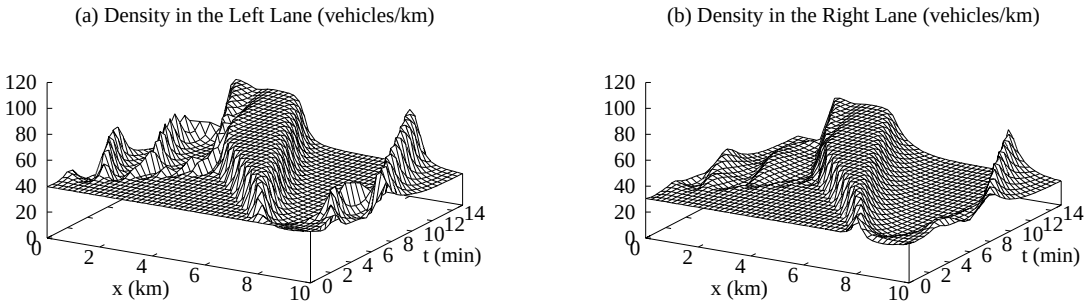

FIG. 15. (a)+(b): Simulation of stop-and-go traffic in the regime of unstable traffic flow, arising from an initial density perturbation in the right lane, which eventually spreads to the left lane. The similarity of the traffic patterns in both lanes indicates synchronization and originates from lane changes which reduce developing disequilibria among lanes. The parameter values used in the above simulation are displayed in Table II.

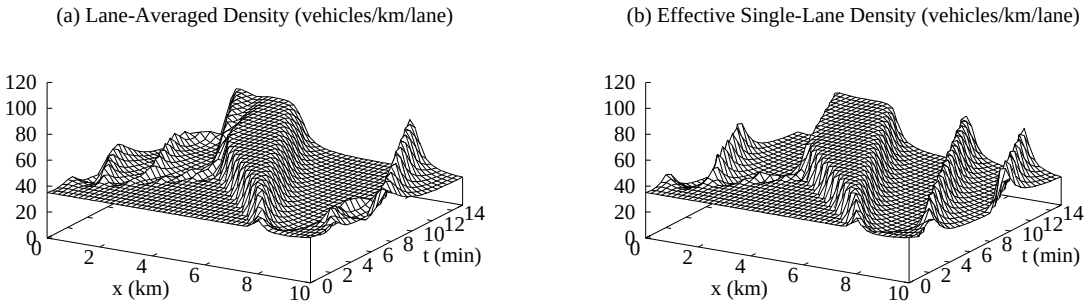

FIG. 16. Comparison of (a) the lane-averaged density according to the multi-lane simulations displayed in Figure 15 and (b) the density resulting from the effective single-lane model of Section III B, using the "effective" model parameters $V_0 = 110\,\mathrm{km/h}$, $\rho_{\max} = 150\,\mathrm{vehicles/km/lane}$, $\tau = 35\,\mathrm{s}$, $T = 1.6\,\mathrm{s}$, $\gamma = 1.2$, $\alpha_0 = 0.007$, $\Delta\alpha = 0.031$, $\rho_\mathrm{c} = 0.28\rho^{\max}$, and $\Delta\rho = 0.025\rho^{\max}$.